PERGAMON

Journal of Structural Geology 23 (2001) 1507–1529

JOURNAL OF STRUCTURAL GEOLOGY

www.elsevier.com/locate/jstrugeo

Calculation of shortening due to outcrop-scale deformation and its relation to regional deformation patterns

James P. Hogan, William M. Dunne*

306 GS Building, University of Tennessee, Knoxville, TN 37996-1410, USA

Received 24 January 2000; accepted 17 October 2000

Abstract

The objectives of this study are to: assess the regional contribution of outcrop-scale structures in well-exposed rocks of a tectonic province; and evaluate how failure to measure this scale of structure affects the assessment of regional deformation. The contribution of outcrop-scale structures to regional deformation has not been quantified previously because of the need for long continuous exposures to regionally characterize the structures. This study used 18.6 km of semi-continuous roadcut and streambed exposures in well-exposed Devonian clastic rocks to construct 1:200-scale profiles to address the objectives.

Key results are: (1) outcrop-scale structures contribute about 1/6 to 1/4 of total regional shortening. (2) Submapscale shortening components from microscale and outcrop-scale structures equal mapscale shortening that would be interpreted from a regional cross-section. (3) Analysis of submapscale structures in the target blind thrust belt is needed to identify that the roof-sequence deformation preceded and continued through duplex formation. (4) The kinematic response of the roof sequence would be incorrectly identified as backthrusting if the shortening contribution of outcrop-scale structures is ignored. (5) Although measured outcrop-scale shortening does not match that predicted by the fractal analysis of other workers, the fractal approach to predicting deformation as a function of scale may still be valid.

Keywords: Shortening; Outcrop-scale deformation; Tectonic province

1. Introduction

The objectives of this study are to: (1) assess the regional contribution of outcrop-scale structures in well exposed rocks of a tectonic province; and (2) evaluate the effect that failure to measure this scale component for deformation has on the assessment of tectonic deformation. In areas of tectonic activity, deformation typically occurs at all scales, ranging from structures in atomic lattices to structures forming mountain ranges (Pumpelly, 1918; Ramsay and Huber, 1983; Kligfield et al., 1984; Onasch and Dunne, 1993; Wu, 1993; Mitra, 1994; Holl and Anastasio, 1995; Smart et al., 1997). Three scales of observation are commonly used to describe the structures: microscale ($<$0.01 m), outcrop scale (0.01–100 m), and mapscale ($>$100 m) (Hancock, 1985; Mitra, 1994; Smart et al., 1997).

The typical scale for considering deformation in a tectonic province is mapscale. For example, the three-dimensional geometry of a tectonic province is often illustrated by combining surface and subsurface data to construct cross-sections that may be retrodeformable (e.g. Laubscher, 1962; Dahlstrom, 1969; Hatcher, 1981; Roeder and Witherspoon, 1978; Boyer and Elliott, 1982; Dixon, 1982; Wernicke and Burchfiel, 1982; Woodward, 1985; Allmendinger, 1992; Wernicke, 1992; Wilson and Shumaker, 1992; Epard and Groshong, 1993). Unfortunately, most such regional cross-sections only incorporate mapscale structures and fail to include smaller structures that typically accommodate additional deformation.

The significance of this study revolves around the question: when assessing regional deformation magnitude, such as across an entire thrust belt, is it necessary to consider submapscale, particularly outcrop-scale, structures? Researchers are commonly discouraged from assessing submapscale structures given the laborious procedures for measuring these features (e.g. Groshong, 1972; Ramsay and Huber, 1983; Wojtal, 1986; 1989). Also, for outcrop-scale structures, long continuous exposures are needed to provide a representative sample (Williams, 1970). Thus, it has been easier to incorporate only mapscale analysis into understanding the deformation of a tectonic province. Over the years, various investigators have shown that smaller-scale structures do make a significant contribution to total

* Corresponding author.
E-mail address: wdunne@utk.edu (W.M. Dunne).

0191-8141/01/$ - see front matter
PII: S0191-8141(01)00016-5

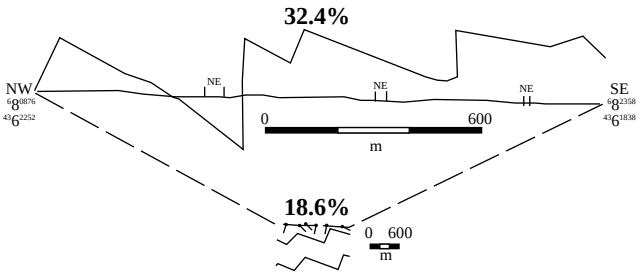

Fig. 1. Profile for difference in measured shortening by changing sampling scale: 18.6% for part of a regional section constructed at 1:37,500 versus 32.4% from a profile constructed at 1:3,000. NE = No exposure; Universal Transverse Mercator projection system (after Johnston, 1989).

deformation, but the majority of these analyses considered the contribution of only microscale structures or isolated outcrop-scale structures (e.g. Cloos, 1947; 1951; Ramsay, 1981; Reks and Gray, 1983; Kligfield et al., 1984; Burgmann, 1991; Evans and Dunne, 1991; Mitra, 1994; Smart et al., 1997; Tavarnelli and Holdsworth, 1999).

An example of the importance of including microscale data in the analysis of a tectonic province is provided by Mitra (1994). Strain was measured in sections parallel to the transport direction across the Sevier fold-and-thrust belt (Idaho–Utah–Wyoming). Mitra demonstrated that failure to include microscale deformation in the restoration of regional cross-sections introduced two errors of tectonic significance: (1) overestimation of the wedge taper for the thrust belt by 3°, and hence, (2) underestimation of the mechanical strength of rocks within the wedge at the time of deformation (Mitra, 1994). Another study did examine the contribution of both microscale and outcrop-scale data to regional deformation using the foreland thrust belt of the central Appalachians (Smart et al., 1997). They demonstrated that failure to include smaller structures would miss more than 75% of shortening in the roof sequence of this blind thrust belt, and would also lead to an incorrect mapscale evaluation that the roof sequence moved into the hinterland over duplexes rather than into the foreland in front of the duplexes. Still, this study was only able to include outcrop-scale structures on a spot basis because of the lack of continuous exposure. Consequently, an important issue remains unresolved: are these spot samples representative of outcrop-scale structural geometry and abundance across a regional structure?

Other studies have used outcrop-scale structures to examine kinematic behavior and deformation processes (e.g. Cloos, 1951; Williams, 1970; Nickelsen, 1979; Simon and Gray, 1982; Scott and Dunne, 1990; Stanley, 1990; Stewart and Hancock, 1991; Kattenhorn and McConnell, 1994; Ferrill et al., 1998), but once again, the lack of long continuous exposures has precluded evaluating whether these informative geometries are representative on a regional scale. The use of several long continuous exposures allows

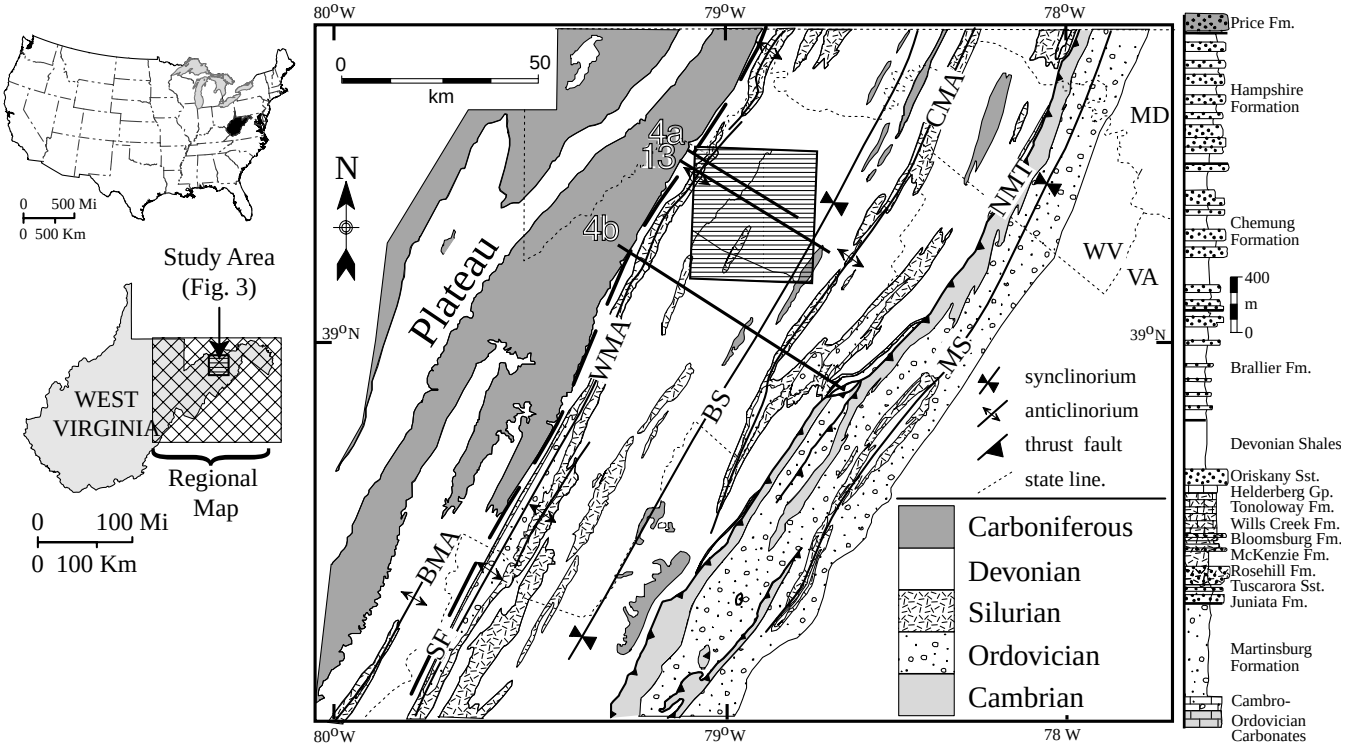

Fig. 2. Geologic map of central Appalachian Valley and Ridge and Plateau provinces with stratigraphic column. BMA = Browns Mountain anticlinorium; SF = Alleghany structural front; WMA = Wills Mountain anticlinorium; BS = Broadtop synclinorium; CMA = Cacapon Mountain/Adams Run anticlinorium; NMT = North Mountain thrust; MS = Massanutten synclinorium; 4a, 4b, and 13 are figure numbers for cross-section locations; hachured box is location of this map; striped box is location of Fig. 3.

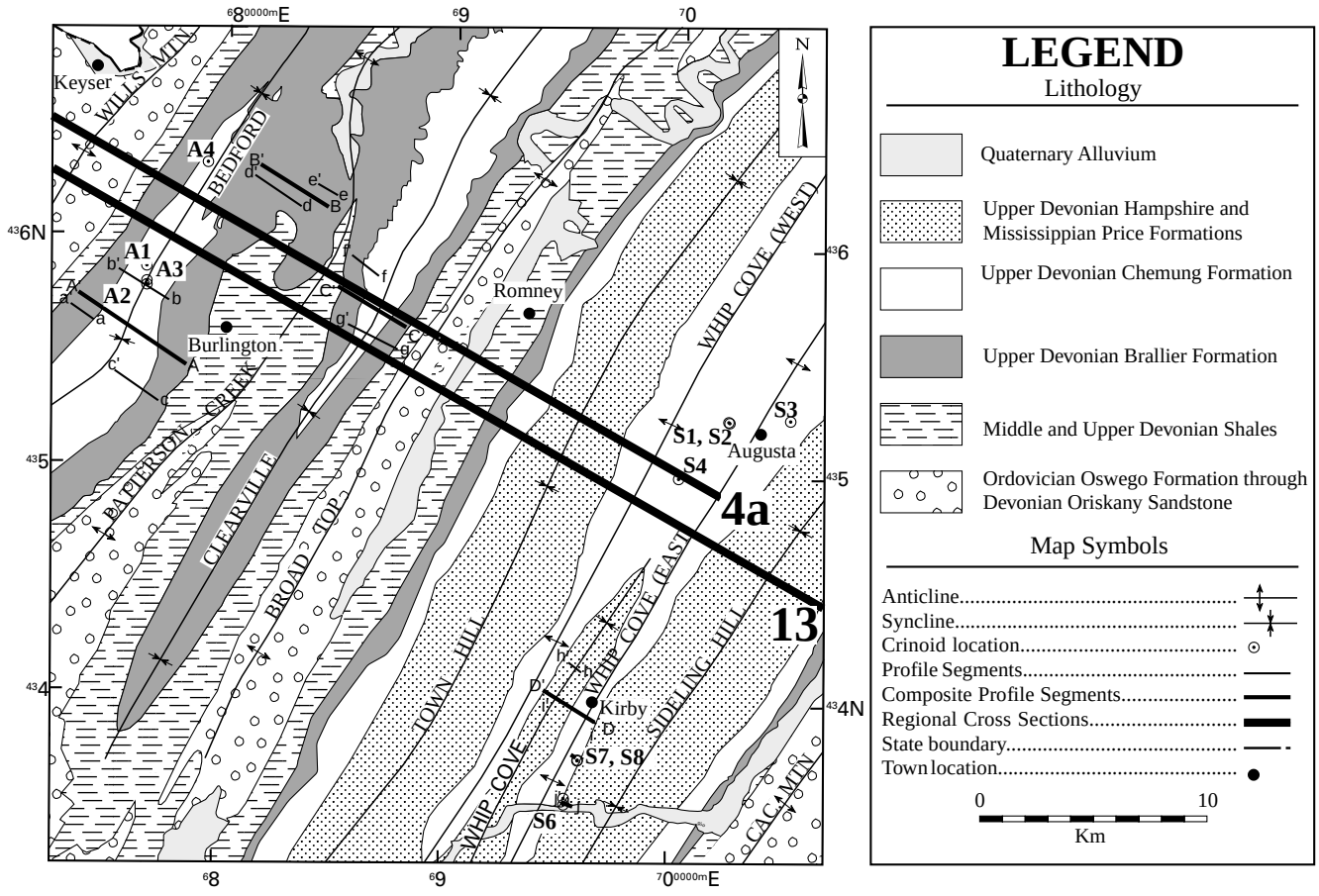

Fig. 3. Geologic map of study area (see Fig. 2 for location). Profiles, composite profiles, and regional cross-sections are denoted by lower-case letters, capital letters, and numbers, respectively. Crinoid samples from Appendix C (NOTE: Sample S5 is located in the Sideling Hill syncline along strike to the northeast, west of Augusta). 4a and 13 are cross-section locations. Wills Mtn. = Wills Mountain anticline; Cac. Mtn. = Cacapon Mountain anticline. UTM coordinates (after Cardwell et al., 1968; Schultz, 1995; U.S. Geological Survey, 1998).

the typical characteristics of outcrop-scale structures to be determined, and minimizes exposure gaps, which reduces the risk that the gaps contain systematically greater or lesser structural complexity than exposed features.

Johnston (1989) conducted a pilot study in the central Appalachian foreland that indicated the potential for this part of a thrust belt to be a natural laboratory for assessing the contribution of outcrop-scale structures to regional deformation (Fig. 1). He used a near-continuous exposure exceeding 1.5 km in length that showed a 43% error in shortening if outcrop-scale structures were not incorporated into the analysis. Another indication that submapscale structures may have a significant role in the regional deformation of the central Appalachian portion of the Alleghanian foreland thrust belt comes from a fractal analysis of mapscale folds in a regional cross-section (Wu, 1993, 1995). Wu used a compass methodology to argue that sequences with folding at many scales, instead of just mapscale, will have a higher fractal dimension for the complexity of folded layer shapes. From this premise, he predicted that structures, particularly folds, with sizes less than 50 m would account for about 60% of the total shortening (24% absolute shortening) in the Devonian and Silurian rocks of this same roof sequence. One concern about this prediction is that the measurement methodology does not incorporate discontinuous structures such as cleavage or subgrain scale structures, which could be prevalent below the centimeter scale (Dunne and Ferrill, 1995). Nonetheless, Wu's prediction indicates the possibility of a significant submapscale shortening contribution in roof-sequence rocks of the central Appalachians. Based on Johnston's successful test and Wu's prediction, we decided to use a series of long near-continuous profiles in the central Appalachians foreland to examine the role of outcrop-scale structures in regional deformation.

2. Geologic setting

This study was conducted in the western Valley and Ridge province of the central Appalachians, which is bound by the North Mountain thrust to the east and the Alleghanian structural front and Appalachian Plateau to the west (Fig. 2). Three structures dominate the surface

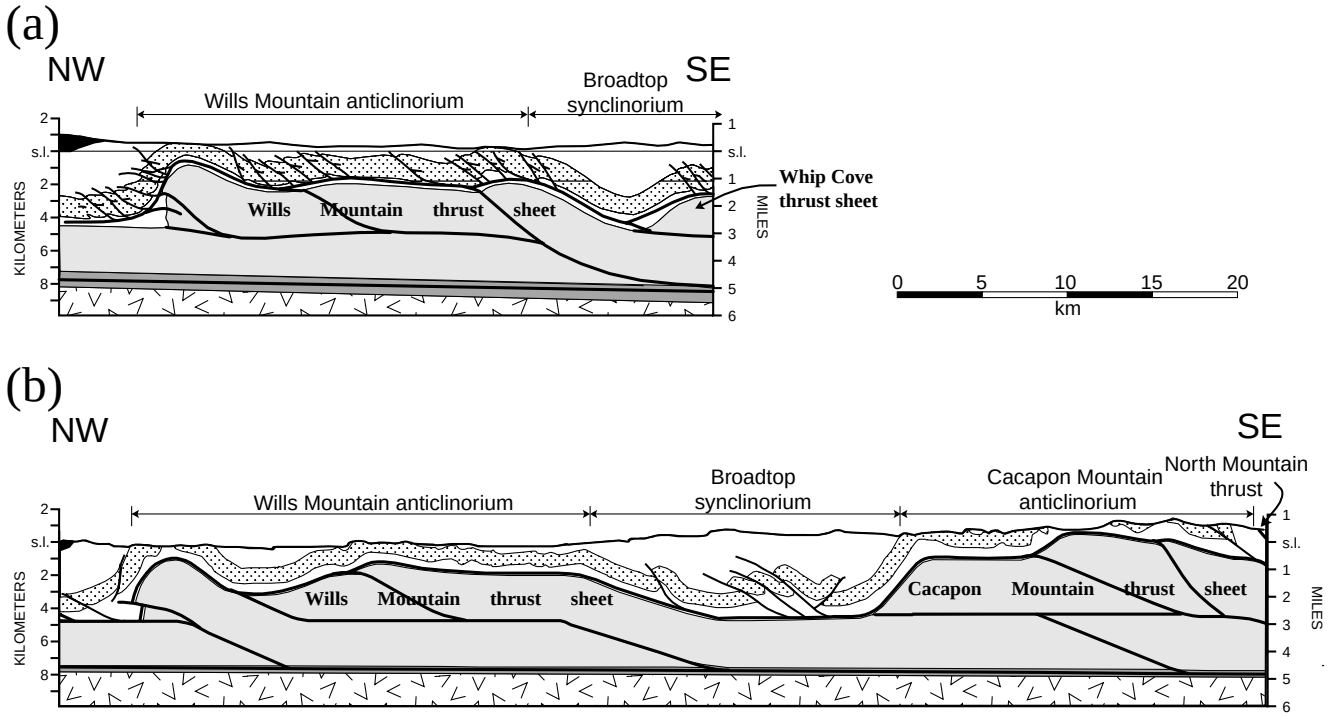

Fig. 4. Regional cross-sections: (a) modified from line 2 in Wilson and Shumaker (1992); (b) modified from Dunne (1996). Locations in Fig. 2. Black = Pennsylvanian and Mississippian; white = middle and upper Devonian; dots = Ordovician Oswego Formation through Devonian Oriskany Sandstone; stippled = Ordovician Martinsburg Formation; light gray = Cambrian–Ordovician carbonates; dark gray = Cambrian Waynesboro Formation; v-pattern = Lower Cambrian, Precambrian basement; thick black lines = thrust faults in Cambro–Ordovician carbonates; thin black lines = thrust faults in Martinsburg Formation.

geology of this area: the Wills Mountain anticlinorium, Broadtop synclinorium, and Cacapon Mountain anticlinorium (Figs. 2 and 3). The anticlinoria are underlain by duplexes of Cambro–Ordovician carbonates (Perry, 1971, 1978a; Jacobeen and Kanes, 1974; Kulander and Dean, 1986; Mitra, 1986; Evans, 1989; Wilson and Shumaker, 1992) (Fig. 4a and b). Thus, the surface rocks are part of the roof sequence for this Alleghanian blind foreland thrust belt (Gwinn, 1964, 1970; Rodgers, 1970; Geiser, 1988a; Dunne, 1996).

The target stratigraphic units for this study are the Upper Devonian Brallier and Chemung Formations (Figs. 2 and 3). The Brallier Formation consists of thin-bedded clastic sedimentary rocks, and has a thickness of about 610 m (2000′) (Reger and Tucker, 1924; Tilton et al., 1927; Dennison and Naegele, 1963; Schultz, 1995). The Chemung Formation also consists of thin-bedded clastic sedimentary rocks, totaling about 460 m (1500′) (Reger and Tucker, 1924; Tilton et al., 1927; Dennison and Naegele, 1963; Schultz, 1995). The Brallier Formation grades upward into the Chemung Formation, which is distinguished by thicker and more abundant sandstone beds, some of which contain marine fossils (Reger and Tucker, 1924; Tilton et al., 1927; Dennison, 1963; 1971; Dennison and Naegele, 1963; Dennison et al., 1988; Schultz, 1995). Detailed structural analyses and stratigraphic examinations during this study identified several errors with previous regional geologic maps concerning the location of the upper and lower contacts of the Chemung Formation. For example, all the composite profile D–D′ lies within the Brallier and Chemung Formations based on field work, but Fig. 3 shows that this profile should be located in the Hampshire Formation, which is defined by red beds of sandstone and shale.

The two stratigraphic units provide two key advantages for this study. First, they are in long continuous exposures through both the Wills Mountain anticlinorium and Broadtop synclinorium, providing a sample above a duplex with complete stratigraphic duplication and significant displacement (Wills Mountain thrust sheet) and a duplex with partial duplication and much less displacement (Whip Cove thrust sheet), respectively (Fig. 4a). Second, the two units contain similar clastic lithologies and structures through both of these tectonic positions, providing comparable features for analysis at all locations in rock units that probably behaved in a very similar mechanical manner.

The Upper Devonian clastic rocks in the study area are dominated by folds with angular to rounded hinge shapes, generally planar limbs, and open to tight interlimb angles (Fig. 5a–d). Larger synclines more commonly have rounded hinges (Fig. 5c), whereas anticlines have more angular hinges (Fig. 5d), but, overall, folds typically have narrow hinge zones and straight limbs. Homoclinal bedding also occurs for long stretches of exposure along mapscale

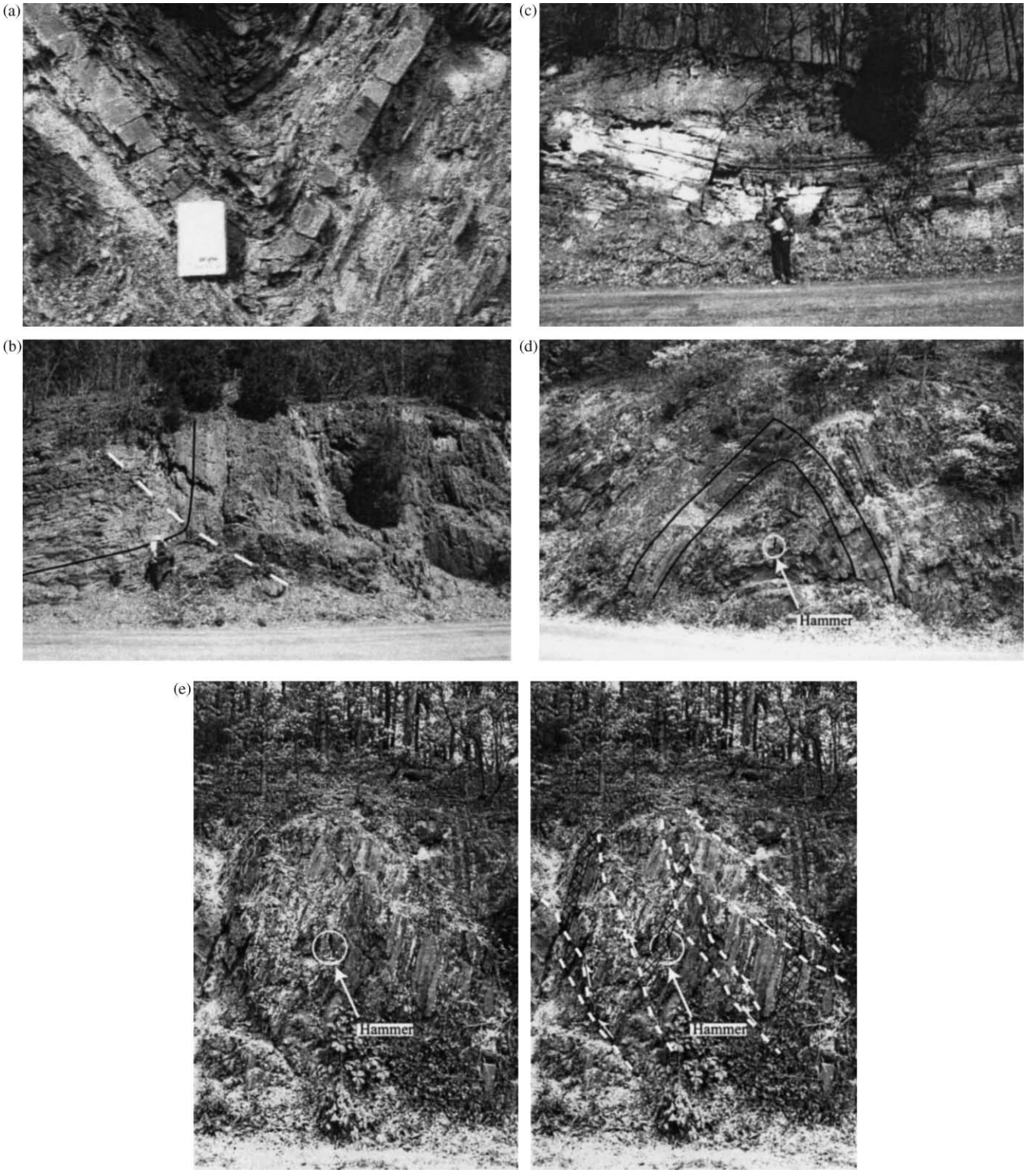

Fig. 5. Outcrop structural style along roadcuts and steambeds. See profile locations in Fig. 3. (a) Subangular fold along profile a–a′ (fieldbook for scale). (b) Dip-domain boundary (white dashed line) dividing vertical beds to right of person from gentle northwest-dipping beds to left along profile d–d′ (person for scale). (c) Open synclinal hinge along profile d–d′ (person for scale). (d) Whip Cove anticline (East) hinge along profile i–i′ (rock hammer for scale). (e) Outcrop-scale faults (white dashed lines) along profile i–i′ east of Fig. 6d (rock hammer for scale); hachured marker beds show offsets.

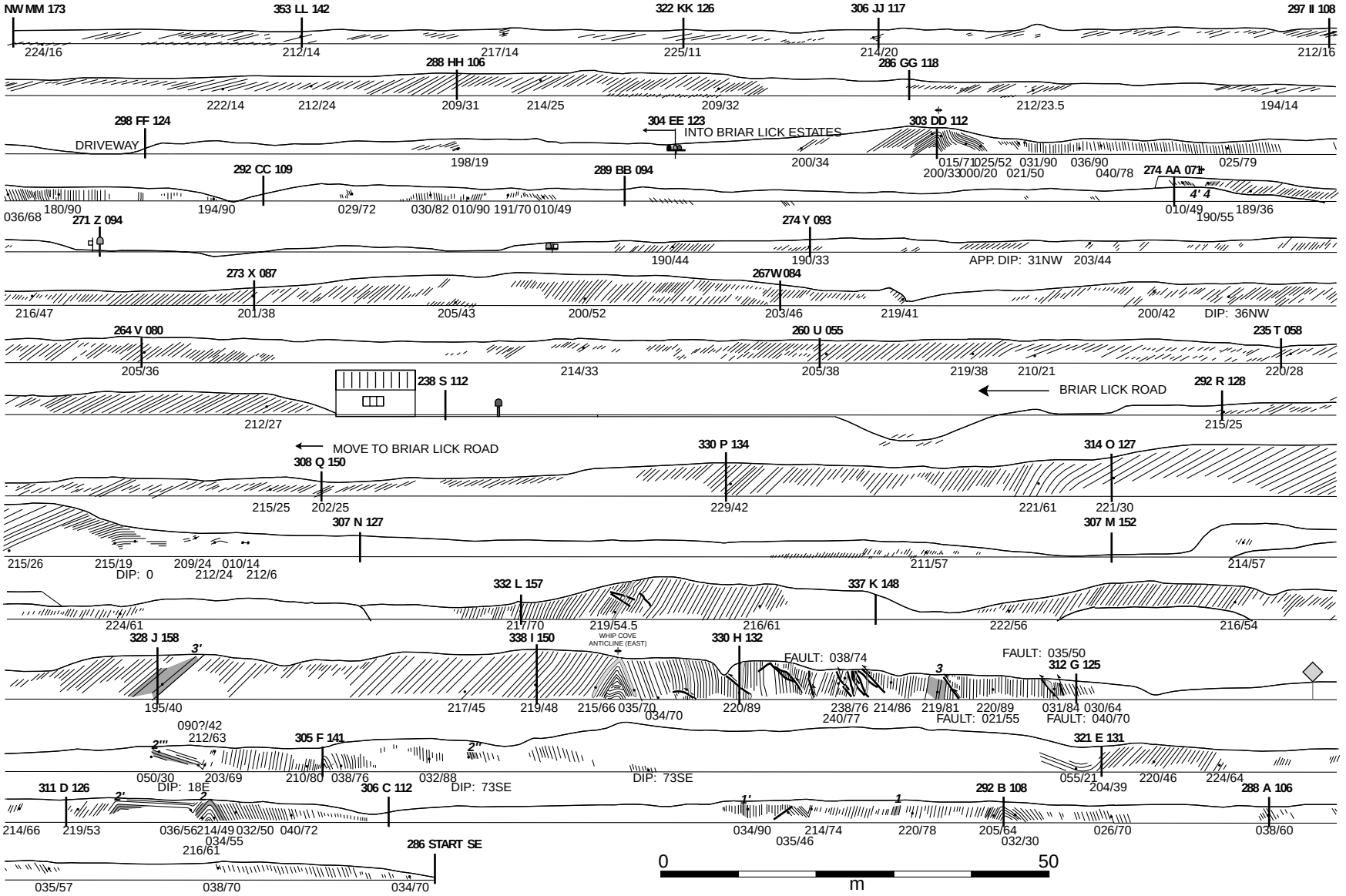
NW MM 173
353 LL 142
322 KK 126
306 JJ 117
297 II 108
224/16
212/14
217/14
225/11
214/20
212/16
288 HH 106
286 GG 118
222/14
212/24
209/31
214/25
209/32
212/23.5
194/14
298 FF 124
DRIVEWAY
304 EE 123
INTO BRIAR LICK ESTATES
303 DD 112
198/19
200/34
015/71 025/52 031/90 036/90 025/79
200/33 000/20 021/50 040/78
292 CC 109
289 BB 094
274 AA 071
4' 4
036/68 180/90
194/90
029/72
030/82 010/90 191/70 010/49
010/49 189/36
190/55
271 Z 094
274 Y 093
190/44
190/33
APP. DIP: 31NW 203/44
273 X 087
267W 084
216/47
201/38
205/43
200/52
203/46
219/41
200/42
DIP: 36NW
264 V 080
260 U 055
235 T 058
205/36
214/33
205/38
219/38
210/21
220/28
238 S 112
BRIAR LICK ROAD
292 R 128
212/27
215/25
MOVE TO BRIAR LICK ROAD
330 P 134
314 O 127
308 Q 150
215/25
202/25
229/42
221/61
221/30
307 N 127
307 M 152
215/26
215/19
209/24 010/14
DIP: 0
212/24 212/6
211/57
214/57
332 L 157
337 K 148
224/61
217/70
219/54.5
216/61
222/56
216/54
328 J 158
3'
338 I 150
WHIP COVE ANTICLINE (EAST)
330 H 132
FAULT: 038/74
FAULT: 035/50
3
312 G 125
195/40
217/45
219/48
215/66 035/70
034/70
220/89
238/76 214/86 219/81 220/89 031/84 030/64
240/77
FAULT: 021/55
FAULT: 040/70
090?/42
212/63
2'''
305 F 141
2''
321 E 131
050/30
203/69
210/80 038/76
032/88
DIP: 18E
DIP: 73SE
DIP: 73SE
055/21
204/39
220/46
224/64
311 D 126
2'
2
306 C 112
1'
1
292 B 108
288 A 106
214/66
219/53
036/56 214/49 032/50 040/72
034/55
216/61
034/90
035/46
214/74
220/78
205/64
032/30
026/70
038/60
286 START SE
035/57
038/70
034/70
0
50
m

structures (Figs. 6 and 7). Fold axes plunge zero to a few degrees, and axial surfaces generally dip southeast, but northwest-dipping axial surfaces do exist (Schultz, 1995).

Although predicted to be abundant (Kulander and Dean, 1986; Wilson and Shumaker, 1992), evidence for mapscale faults was not found either in the form of fault zones or stratigraphic mismatches across intervening patches of no exposure in the 18.6 km of measured profiles (Table 1). This lack of mapscale faults is consistent with previous observations from the synclinorium and a regional deformation assessment for the roof sequence (Schultz, 1995; Dunne, 1996). Based on these observations and previous work, no mapscale faults are thought to exist within the profiles. Groups of outcrop-scale faults were found in only two 20 m zones, which show offsets of bedding on the scale of centimeters to meters (Fig. 5e). They occur where folds are abundant and tight along Grassy Lick Road (i–i′) (Fig. 6) and Parker Road (g–g′) (Fig. 7).

Two of the nine profiles used for outcrop-scale analysis are presented here in the main text (Figs. 6 and 7) and the other seven are available in Hogan (2000). As previously mentioned, long continuous exposures are preferred for conducting the outcrop-scale analysis, whereas the 18.6 km of profile length for this study averaged about 66% exposure (Table 1), but the lack of 100% exposure can be overcome so long as marker beds can be traced through exposure gaps (Williams, 1970). For example, profiles g–g′ and i–i′ are two of the three least-exposed profiles (Table 1), yet it is still possible to correlate bedding across most gaps (Figs. 6 and 7).

3. Strain assessment

3.1. Outcrop and mapscale

Construction of detailed profiles along well-exposed roadcuts and streambeds generated the key new data set for this study. The roadcuts and streambeds are perpendicular or sub-perpendicular to strike and are of sufficient length collectively to provide a regional sample.

A five-step procedure was used to construct profiles and then produce composite profiles (Fig. 8). First, profile lines were surveyed using a tape-measure and compass (Fig. 8a). Second, detailed profiles were constructed along the surveyed line at 1:200 by sketching marker beds and structures while recording structural orientation. Third, these field sketches were compiled as continuous profiles at 1:750 in Adobe Illustrator 8.0® files (Figs. 6 and 7).

In the fourth step, a projection line normal to regional strike was selected through each profile, and profile data were projected to construct the overall structural geometry normal to strike (Fig. 8b) (Donn and Shimer, 1958). For the folds where plunge was calculated ($\geq 1°$), fold axes were projected using the down-plunge projection technique (Mackin, 1950). For each profile, a single line was constructed using dip domains, primarily because most folds have straight limbs with narrow hinge zones (Fig. 8b) (Faill, 1969, 1973; Laubscher, 1977; Suppe, 1983). However, where curved broad hinges exist, a parallel fold construction was used (Dahlstrom, 1990). A single line was used in each profile to simply illustrate the structural geometry and to feature the different sized structures.

Finally, in the fifth step, geographically close profiles were projected onto a single plane normal to strike to construct 1:7500 composite profiles (Figs. 4, 8c and 9). These composite profiles are the regional-size samples for this analysis. Three composite profiles are in the Wills Mountain anticlinorium and one is in the Broadtop synclinorium (Figs. 4 and 9; Table 2).

Field data include second (2.5–3 km wavelength) through fourth-order (1–50 m wavelength) folds (Nickelsen, 1963). Third- and fourth-order folds and outcrop-scale faults are smaller than 250 m in size, and often will not project laterally into the strike-normal profile due to their limited lateral persistence (Faill, 1969, 1973; Dubey and Cobbold, 1977). Consequently, lateral projection would eliminate many smaller structures. To preserve the deformation represented by these smaller structures, it was assumed that they were representative. Therefore, they were literally projected into strike-normal profiles and subsequent composite profiles where the exact position of these smaller structures is not known. The identification of 146 small folds and a few faults in 18.6 km of 1:200 profiles is interpreted to provide a representative sample of their abundance and geometry for the 1:7500 composite profiles. Hence, we believe that the literal projection of these smaller structures is an appropriate method to approximate their contribution to regional deformation. Also, this projection technique favored the construction of a single line along bedding rather than a complete cross-section, so as to eliminate the need to derive a strategy for determining the areal distribution of these smaller folds in a section.

Where exposure gaps occur along lines, it was assumed that the two bounding dips of beds could be used to construct two separate lines to show the maximum and minimum amounts of profile shortening. At each gap, shortening was maximized by placing the dip-domain boundary at the end of the gap with the lower bedding dip, implying that the gap was filled by the more steeply dipping rocks and vice versa for minimum shortening. This procedure was used for all gaps, so two lines showing

Fig. 6. Structural data collected along Grassy Lick Road for projection into profile i–i′ (see Fig. 3 for profile location). Thin black lines = layering; thick black lines = faults; dots = location of bedding orientation; numbers below outcrop = bedding orientations using right-hand rule (fault orientations where indicated); dark gray fill = marker beds; bold font above outcrop = bearing of roadcut and survey markers.

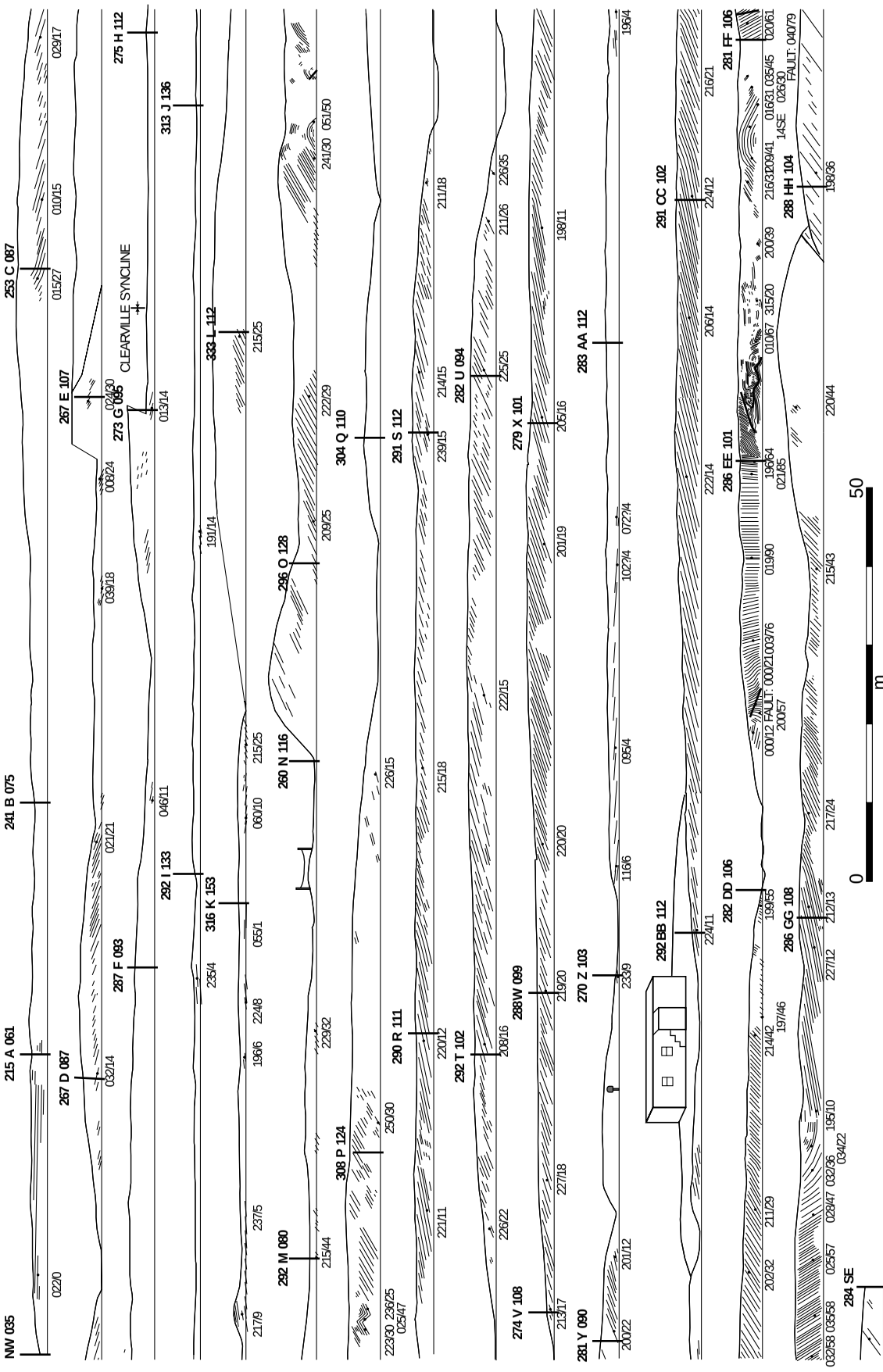

Fig. 7. Structural data collected along Parker Road for projection into profile g–g′ (see Fig. 3 for profile location). See Fig. 6 caption for format.

Table 1
Profile exposure percentages. See Fig. 3 for profile locations

Profile	Section name	Profile length (m)	Exposure (m)	No exposure (m)	Exposure percentage (%)
a–a′	US50	1299	1120	180	86.2
b–b′	Dry Run Road	3102	1991	1111	64.2
c–c′	Shirley Lane Road	2573	1599	974	62.1
d–d′	Beaver Run Road-West	2812	2113	699	75.1
e–e′	Beaver Run Road-East	1252	985	266	78.7
f–f′	Tony Cook Road	1518	941	577	62.0
g–g′	Parker Road	2851	1584	1267	55.6
h–h′	Grassy Lick Road-Gas	755	409	346	54.2
i–i′	Grassy Lick Road	2452	1485	967	60.6
	Total:	18,614	12,227	6387	65.7

structures were constructed across entire profiles and then incorporated into composite profiles (l_{maxo+m}, l_{mino+m}) (Fig. 9). This approach to handling exposure gaps does not allow for the existence of complex structures in the gaps, although, where present, unique stratigraphic packages were projected across gaps and matched on the other side. For example, east of the Whip Cove anticline (East) in Fig. 6, third- and fourth-order folds and outcrop-scale faults are abundant. The presence of a local abundance of smaller structures followed by unexposed section might be interpreted by some as evidence for a mapscale fault. Yet, a 4–5 m sequence of 50–100-cm-thick sandstone and siltstone beds on the southeastern limb of the anticline (west of survey marker 'G', Fig. 6), when projected across the anticline, is matched on the northwestern limb with a similar 4–5 m sequence (survey marker 'J', Fig. 6). This lithologic match precludes mapscale faults from having a significant role in the unexposed stretch.

Having projected smaller structures literally and established stratigraphic continuity where possible across exposure gaps, a pair of bed-parallel lines (l_{maxo+m}, l_{mino+m}) for each composite profile were compared to establish the difference in shortening estimates provided by them. The differences range from 0.7% (profile A–A′; Fig. 9, Table 2) to 7.3% (profile D–D′, Fig. 9, Table 2). These differences are significant enough that the two sets of values were retained for all shortening calculations.

To identify the shortening component related to outcrop-scale structures, mapscale lines were constructed in the composite profiles (Fig. 9) to filter out smaller structures that would not be present in regional cross-sections. Inspecting the available regional cross-sections for the foreland thrust belt of the central Appalachians (Cardwell et al., 1968; Weaver, 1968; Gwinn, 1970; Socolow, 1980; Hatcher, 1981; Woodward, 1985; Kulander and Dean, 1986; Mitra, 1986; Geiser, 1988a; Evans, 1989; Dunne, 1996), folds with wavelengths of smaller than 500 m and faults with displacements of less than 500 m are generally absent. Therefore, structures below this size were not included in mapscale lines for this study. Instead, they were included in the contribution to outcrop-scale shortening. As some of these structures are larger than those typically assumed to be outcrop-scale (<100 m in length dimension; Hancock, 1985), one's first choice might not be to group them with outcrop-scale structures, but they exist, are absent in regional analyses, are found with detailed field work, and will be included here with outcrop-scale structures.

The amount of mapscale shortening was determined by subtracting the line length for the mapscale lines from the deformed-length of the profile:

$$\Delta l_{maxm} = l_{maxm} - l_1 \text{ or } \Delta l_{minm} = l_{minm} - l_1 \quad (1)$$

where l_{maxm} and l_{minm} are maximum and minimum line-lengths of mapscale structures, and l_1 is the present deformed-state length (Fig. 9, Table 2). The magnitude of mapscale shortening in the anticlinorium decreases to the southeast from the Wills Mountain anticline to the Broadtop anticline (Table 2; Figs. 3 and 9). For the synclinorium, mapscale shortening accounts for about 1/2 of the total shortening in profile D–D′ (Table 2; Fig. 9).

The amount of outcrop-scale shortening was determined by subtracting the line length for the mapscale lines from the outcrop-scale lines:

$$\Delta l_{maxo} = l_{maxo+m} - l_{maxm} \text{ or } \Delta l_{mino} = l_{mino+m} - l_{minm} \quad (2)$$

where Δl_{maxo} and Δl_{mino} are maximum and minimum outcrop-scale shortening estimates, l_{maxo+m} and l_{mino+m} are maximum and minimum line-lengths of outcrop plus mapscale structures, and l_{maxm} and l_{minm} are maximum and minimum line lengths of mapscale structures (Fig. 9, Table 2). In profiles B–B′ and C–C′, outcrop-scale shortening is greater relative to the line for l_{minm} because that line has a poorer fit to the outcrop-scale structures than the line for determining l_{maxm} (Fig. 9, Table 2).

Based on the three Wills Mountain anticlinorium profiles, the percentage of shortening from outcrop-scale folds and faults is lowest within the synclinal structures (Bedford syncline and Clearville syncline, Fig. 3), whereas the percentage of shortening is higher west of Patterson Creek Mountain anticline (Table 2). The total outcrop-scale shortening from all three profiles is 1.09–1.12 km, or 6.8–7.2% (Table 2). For the 2.7 km composite profile in the Broadtop synclinorium (Fig. 9), the outcrop-scale shortening above

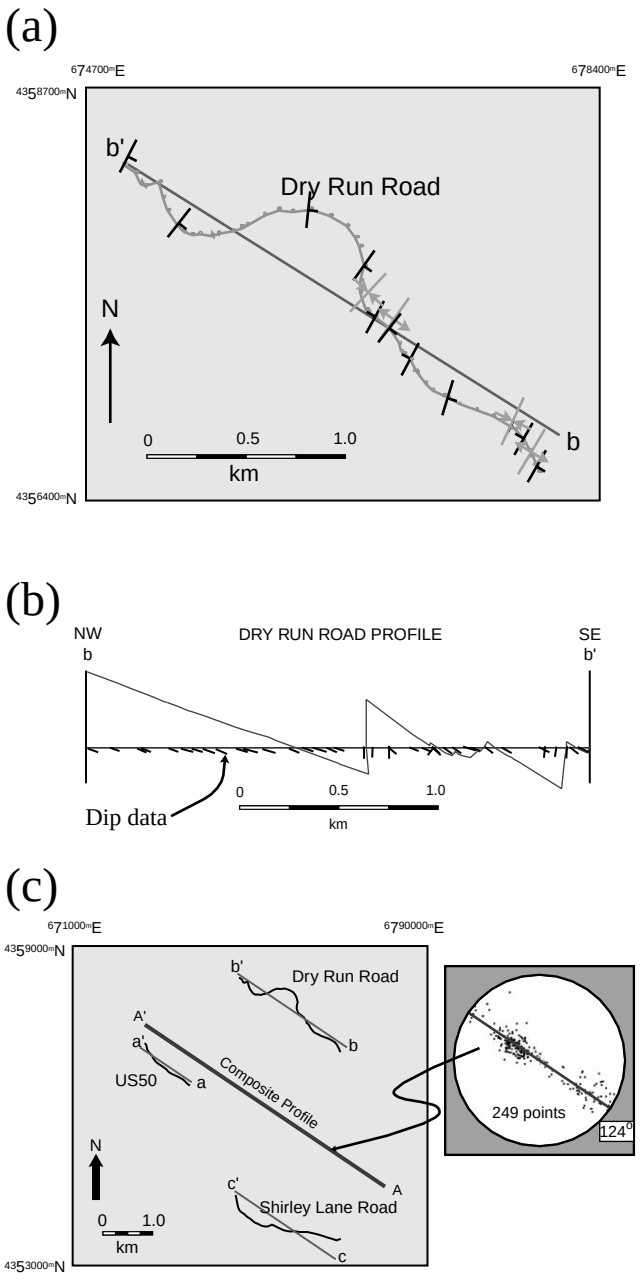

Fig. 8. Profile construction. (a) Map of location of Dry Run Road detailed profile, major fold axes, general dips, and profile line b–b′. (b) Profile b–b′ with projected map-scale folds and outcrop-scale folds placed between them. (c) Map of profiles, a composite profile, and bedding orientation data used for regional projection. Geographic coordinates in UTM.

Whip Cove syncline and Whip Cove anticline (East) in the Broadtop synclinorium is 0.27 km or 5.6% (Table 2). An ideal anticlinorium–synclinorium comparison of roof-sequence rocks would incorporate equivalent amounts of data from each setting, but the shorter width of the outcrop belt for the target stratigraphic units in the synclinorium constrained the data set to 2.7 km in length.

3.2. Microscale

The microscale contribution to regional deformation was determined by collecting 12 samples from crinoid-bearing sandstone beds in the Chemung Formation (Nair, 1992; Smart et al., 1997; Kocher, pers. comm.; Schultz, pers. comm.). The limited number of samples is a result of: (1) the crinoids being restricted in occurrence to the lower Chemung Formation; (2) the need for specimens to be collected in situ; (3) the requirement that ossicles be parallel to bedding for measuring layer-parallel strain (LPS); and (4) a need to acquire a sufficient number of crinoid ossicles per sample. The four specimens from the Wills Mountain anticlinorium and eight from the Broadtop synclinorium were collected on or near the profiles for outcrop-scale deformation (Fig. 3; Appendix A).

The need to collect in situ specimens was made apparent in a previous study from the Plateau and Valley and Ridge provinces in which only 28 of the 193 samples with crinoid ossicles were collected in situ (Nair, 1992; Nair et al., 1995). The justification for using the 165 loose samples was that long axes for the strain ellipses could be assumed to be parallel to bedding strike. Re-analysis of the bedding and long-axis data from the 28 in situ crinoid samples showed that this assumption is not always valid (Fig. 10). The poles-to-bedding lie on a great circle with a strike of 127°, indicating a bedding strike of 027°, but 10 of the 28 in situ samples (36%) yield strain ellipses with long axes that are markedly not strike-parallel.

Each crinoid sample (Fig. 11) was analyzed by taking overlapping images with a digital camera, stitching them together using Enroute Quickstitch 1.02®, and cropping a single image to be linked into Adobe Illustrator®. CadTools 2®, an Adobe Illustrator® plug-in, was used to construct ellipses to measure ossicle shapes and angles. For each ossicle, an axial ratio (R_f) and an angle of the long axis-to-bedding strike (f) was determined. Both the specimen and image were examined simultaneously to prevent erroneous interpretations from image resolution or shadows. The harmonic mean of the R_f values was calculated to determine the strain ratio, R_s, for each specimen (Lisle, 1977; 1985; Ramsay and Huber, 1983). The mean f was determined by averaging f values.

Each ossicle or cast/mold was carefully examined for evidence of deformation. The most common feature was asymmetric preservation of ossicle perimeters, which is interpreted to result from pressure solution (Engelder, 1979a,b). Crinoids were typically deformed during the Alleghanian orogeny in the central Appalachian foreland by a combination of pressure solution and calcite twinning (Engelder, 1979a,b). An earlier examination of twins from near the study area showed that calcite twinning is a minor deformation mechanism (Smart et al., 1997). Given the abundant evidence for solution and the small twin-strains, it was assumed that shortening of ossicles and their surrounding matrix may be approximated by 100% pressure

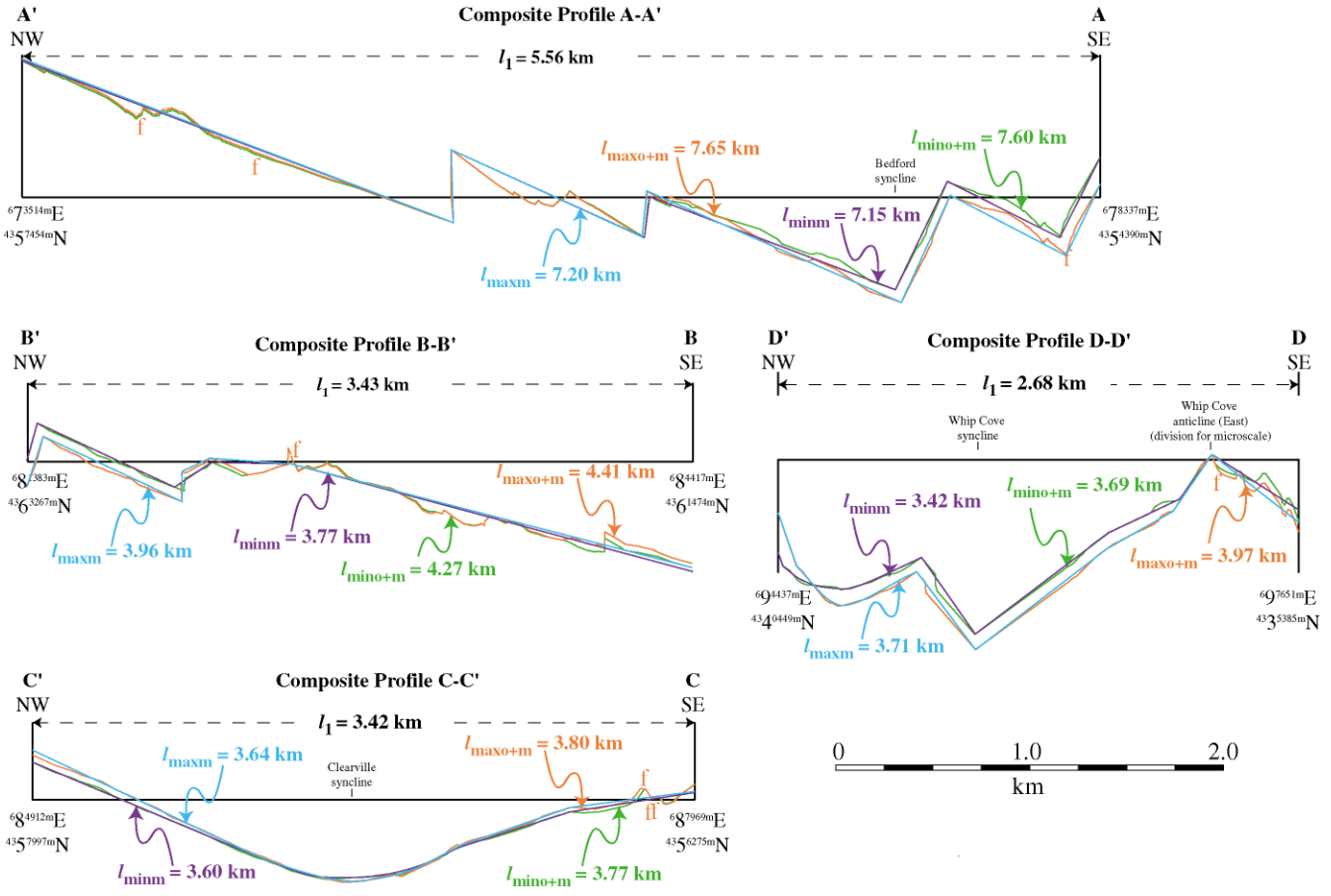

Fig. 9. Composite profiles. See Fig. 3 for locations. l_{maxm} (blue lines) = maximum length of map-scaled structures; l_{maxo+m} (red lines) = maximum length of outcrop plus map-scale structure; l_{minm} (purple lines) = minimum length of map-scale structures; l_{mino+m} (green lines) = minimum length of outcrop plus map-scale structures; red 'f' = fault; ends of composite profiles in UTM coordinates.

solution. Consequently, ossicles are treated as deformed by volume loss in the shortening direction. Therefore, strain ellipse ratios were converted to elongations by (Onasch, 1984):

$$e_{micro} = 1 - (1/R_s) \quad (3)$$

where e_{micro} is the elongation and R_s is the strain ratio. LPS magnitudes range from 4.8–7.4% with an average of 6.1% in the anticlinorium and 7.4–23.7% with a weighted average of 13.7% in the synclinorium (Table 2).

The shortening directions range from 088° to 137° with an average shortening direction of 119 ± 10° in the Wills Mountain anticlinorium and 114 ± 15° in the Broadtop synclinorium (Appendix A). These mean shortening directions are within 10° of the composite profiles trends (Table 2), so LPS magnitudes are treated as having occurred parallel to the profiles.

The elongations for microscale strain were calculated for each profile using:

$$\Delta l_{maxmi} = [l_{maxo+m}/(1.00 - e_{micro})] - l_{maxo+m} \text{ or } \Delta l_{minmi} = [l_{mino+m}/(1.00 - e_{micro})] - l_{mino+m} \quad (4)$$

where l_{maxo+m} and l_{mino+m} are line lengths for the combined mapscale and outcrop-scale shortening (Fig. 9, Table 2). This equation corrects the line length from map- and outcrop-scale measurements for microscale shortening, and subtracts the uncorrected value to yield the line-length change due to only microscale shortening. e_{micro} for profiles A–A′, B–B′, and C–C′ is the average LPS of 6.1% (Table 2). This value is best constrained for profiles A–A′ and B–B′, since crinoid samples were collected near those two profiles (Fig. 3). The value was applied to C–C′ because the Clearville syncline is a syncline above the Wills Mountain thrust sheet like the Bedford syncline for A–A′ and B–B′ (Figs. 3 and 4) (Wilson and Shumaker, 1992). e_{micro} for D–D′ is a weighted average of 13.7% because a cluster of larger strain values are located east of Whip Cove anticline (East) (Fig. 3; Table 2, Appendix A). The weighted average is composed of two components: 20.0% (average of S5S8) from the hinge of the Whip Cove anticline (East) to D, and 12.0% from this hinge to D′ (S1–S4). Using these values for e_{micro}, microscale shortening (Δl_{minmi}, Δl_{maxmi}) for the profiles in the anticlinorium totals 1.02–1.03 km, and for D–D′ in the synclinorium is 0.59–0.63 km (Table 2).

Table 2
Strain and shortening assessment by scale for composite profiles in Fig. 9

Strain partitioned by scale for Wills Mountain anticlinorium						
Map-scale strain Profile	Trend	l_1[a] (km)	l_{maxm} (km)	l_{minm} (km)	Δl_{maxm} (e_{maxm}[b]) km (%[c])	Δl_{minm} (e_{minm}) km (%)
A–A′	124†	5.56	7.20	7.15	1.64 (20.2%)	1.59 (19.6%)
B–B′	119†	3.43	3.94	3.77	0.51 (10.8%)	0.34 (7.4%)
C–C′	120†	3.42	3.63	3.60	0.22 (5.4%)	0.18 (4.5%)
Total (weighted average %):		12.41	14.78	14.52	2.36 (14.0%)	2.11 (12.7%)
Outcrop-scale strain Profile		l_1 (km)	l_{maxo+m} (km)	l_{mino+m} (km)	Δl_{maxo} (e_{maxo}) km (%)	Δl_{mino} (e_{mino}) km (%)
A–A′		5.56	7.65	7.60	0.45 (5.5%)	0.45 (5.6%)
B–B′		3.43	4.41	4.27	0.47 (10.1%)	0.50 (11.0%)
C–C′		3.42	3.80	3.77	0.16 (4.0%)	0.17 (4.2%)
Total (weighted average %):		12.41	15.86	15.64	1.09 (6.4%)	1.12 (6.7%)
Microscale strain Profile		l_1 (km)	$l_{maxo+m+mi}$ (km)	$l_{mino+m+mi}$ (km)	Δl_{maxmi} (e_{maxmi}) km (%)	Δl_{minmi} (e_{minmi}) km (%)
A–A′		5.56	8.15	8.10	0.50 (6.1%)	0.49 (6.1%)
B–B′		3.43	4.70	4.55	0.29 (6.1%)	0.28 (6.1%)
C–C′		3.42	4.04	4.01	0.25 (6.1%)	0.24 (6.1%)
Total (average %):		12.41	16.89	16.66	1.03 (6.1%)	1.02 (6.1%)
Strain partitioned by scale for Broadtop synclinorium						
Map-scale strain Profile	Trend	l_1[a] (km)	l_{maxm} (km)	l_{minm} (km)	Δl_{maxm} (e_{maxm}[b]) km (%[c])	Δl_{minm} (e_{minm}) km (%)
D–D′	123†	2.68	3.71	3.42	1.02 (22.2%)	0.74 (17.2%)
Outcrop-scale strain Profile		l_1 (km)	l_{maxo+m} (km)	l_{mino+m} (km)	Δl_{maxo} (e_{maxo}) km (%)	Δl_{mino} (e_{mino}) km (%)
D–D′		2.68	3.97	3.69	0.27 (5.8%)	0.27 (6.3%)
Microscale strain Profile		l_1 (km)	$l_{maxo+m+mi}$ (km)	$l_{mino+m+mi}$ (km)	Δl_{maxmi} (e_{maxmi}) km (%)	Δl_{minmi} (e_{minmi}) km (%)
D'–WCA (East)[d]			3.17	3.34	0.43 (12.0%)	0.40 (12.0%)
WCA (East)–D			1.00	0.95	0.20 (20.0%)	0.19 (20.0%)
Total (weighted average %):		2.68	4.17	4.29	0.63 (13.7%)	0.59 (13.8%)

[a] Subscripts for different "l" values explained in caption of Fig. 9.
[b] e values are elongations at each scale; e_{maxm}, e_{minm}, e_{maxo+m}, e_{mino+m} are measured from Fig. 9; $e_{maxo+m+mi}$ and $e_{mino+m+mi}$ are calculated using Eq. (3).
[c] Percent absolute shortening calculated with $l_{maxo+m+mi}$, which incorporates all scales of shortening.
[d] WCA (East) = Whip Cove anticline (East).

3.3. Total shortening from three scales of deformation

As is demonstrated with Fig. 9 and Table 2, considering only the mapscale component of deformation in this portion of the central Appalachian foreland thrust belt underestimates total shortening, because it accounts for only 49–53% of the true total (Appendix B, Fig. 12). Incorporating microscale strain yields an important addition as this scale contributes 26–27% of the total. Yet, incorporating the outcrop-scale structures is also necessary as they yield as much as 24%, or close to a quarter of the total shortening across the four composite profiles (Appendix B). Outcrop-scale deformation also plays a role for calculating microscale shortening. Δl_{micro} is calculated from a bedding length, l_{o+m}, that includes both mapscale and outcrop-scale contributions (Eq. (4)). The inclusion of outcrop-scale shortening

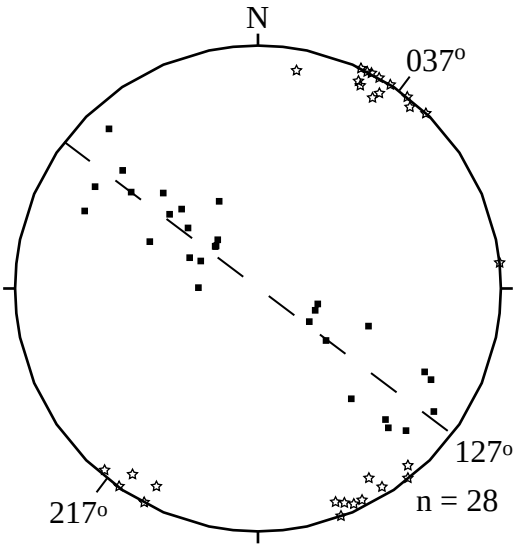

Fig. 10. Equal-area lower-hemisphere stereonet for 28 in situ crinoid specimens from the Valley and Ridge and Appalachian Plateau showing bedding orientations and long axes orientations for calculated strain ellipses (after Nair, 1992). Stars for poles of R_s long axis; solid squares for poles to bedding surfaces; dashed line = calculated best-fit great circle.

increases the base length of all of the profiles for calculating e_{micro} by 1.4 km, and hence, increases the magnitude of e_{micro} by 0.13 km. Consequently, failing to incorporate outcrop-scale structures causes microscale shortening to be underestimated by about 8%.

If one considers the spatial distribution of the shortening contribution from each scale of structure, then mapscale shortening increases northwest across the Wills Mountain anticlinorium (Figs. 3 and 9; Table 2). The increase reflects more abundant mapscale folds approaching the Wills Mountain anticline. At mapscale, the relative shortening contribution in the Broadtop synclinorium falls within the range of values from the profiles in the anticlinorium (Appendix B). The relative contribution of outcrop-scale structures is opposite to that of mapscale structures, with maxima occurring where mapscale values have minima (Appendix B). Yet, in absolute terms, the outcrop-scale structures typically account for 4–6% shortening except for about a 10.5% maximum in B–B′ (Table 2). The relative contribution of microscale structures decreases to the northwest, but more importantly, in absolute terms, the microscale contribution is 2–3 times larger in the synclinorium as compared with the anticlinorium (Table 2, Appendix B).

3.4. Total deformation for a regional cross-section

3.4.1. Assumptions and constraints for cross-section construction

After having determined the relative and absolute strain contributions for different sizes of structure from the 18.6 km sample, the results will be extrapolated to a regional cross-section (Fig. 13) to consider tectonic-scale issues. This extrapolation is done in two stages. First, segments of the section that center on the composite profiles are used to investigate vertical shortening distributions as a function of the degree of duplex duplication. Second, the entire section is examined to consider the regional differences in shortening between roof sequence and duplex. The extrapolations involve qualitatively estimating shortening as a function of structural scale into areas outside those sampled by the profiles. These estimates and their basis will be discussed in the appropriate subsections.

The interpretation of the extrapolations depends on the macroscale geometry portrayed in the regional cross-section, particularly for the underlying duplex of Cambro–Ordovician carbonates (Fig. 13). Constraints for section construction are: (1) surface geology from both existing maps and new mapping during this project; (2) new stratigraphic and bedding orientation data; (3) stratigraphic thickness data from previous work; (4) published seismic reflection data for the Wills Mountain structures particularly; and (5) depth and dip of basement from extrapolating through flatlying stratigraphy in the adjacent Appalachian Plateau and interpretation of published seismic reflection data (Reger and Tucker, 1924; Tilton et al., 1927; Dennison and Naegele, 1963; Perry, 1978a; Evans, 1989; Wilson and Shumaker, 1992; Schultz, 1995). In this interpretation, the thickness of the decollement horizon for the duplex, the Martinsburg Formation, is allowed to vary, whereas overlying and underlying units generally preserve bed-normal thickness. These units consistently display this behavior at the mapscale in the field, whereas the thickness variation of the Martinsburg Formation is not well understood. While the formation is generally considered to be very weak and to support flats with up to 60 km of displacement (Evans, 1989), its fine-grained, dark-colored rocks with much deformation have proved enigmatic to field mappers.

While details of duplex geometry may not be uniquely derivable from the existing constraints, the key characteristics are. For the purposes of the following discussion, the key characteristics are the complete duplication of the Wills Mountain thrust sheet and the horses on the eastern edge of the section, and the partial duplication of the Whip Cove thrust sheet. These geometries control the amount and distribution of the mapscale shortening in the duplex and are well documented by published seismic reflection data (Mitra, 1986; Evans, 1989; Wilson and Shumaker, 1992). Also, macroscale Alleghanian thrusting is assumed to have proceeded into the foreland, which is consistent with previous work (Perry, 1978a; Marshak and Engelder, 1985; Mitra, 1986; Geiser, 1988a; Wilson and Shumaker, 1992; Dunne, 1996). Therefore, only small variations exist in the magnitude of interpreted mapscale shortening from the regional cross-section, because the primary elements are correctly identified, making interpretation of the extrapolations valid.

The extrapolations are performed at the contact between

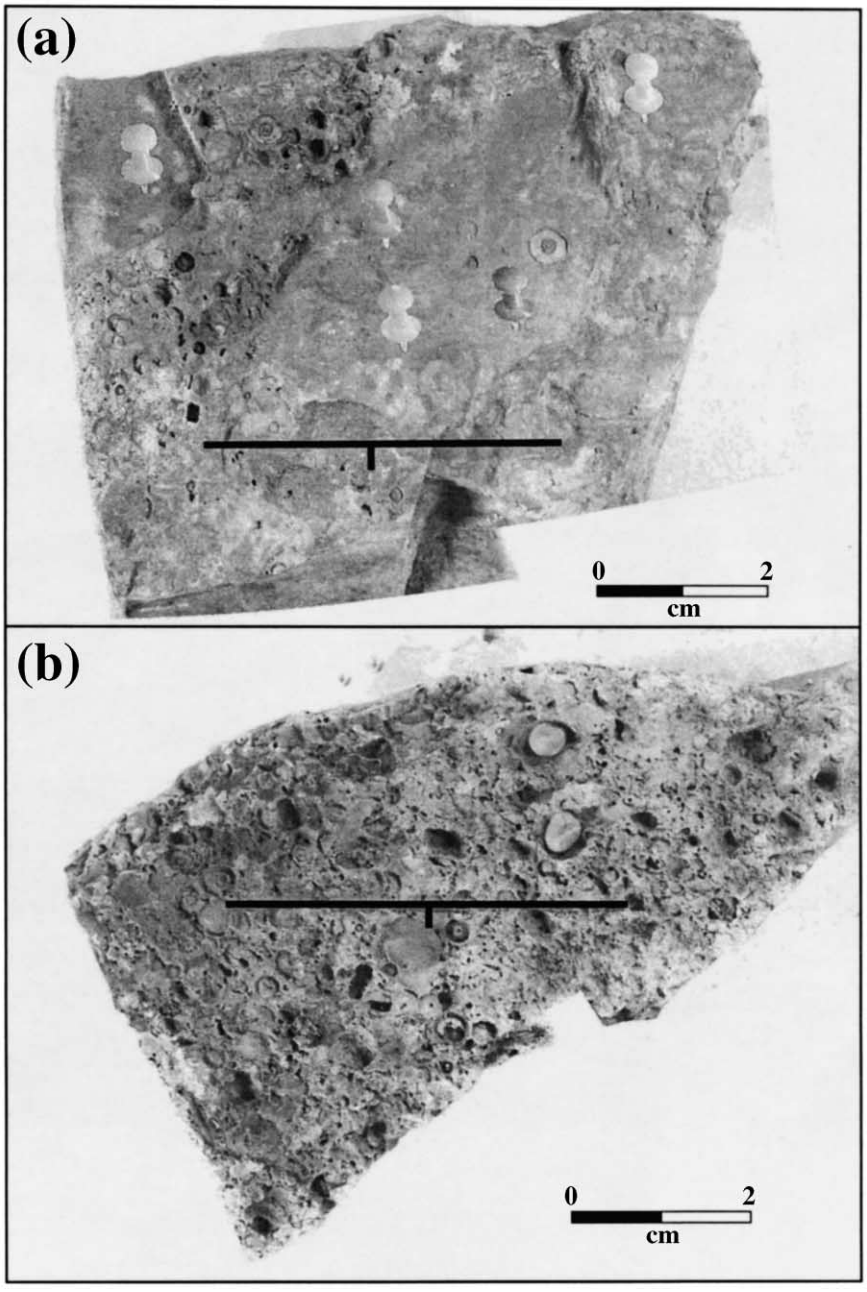

Fig. 11. Chemung Formation samples with crinoid ossicles on bedding surface. See Fig. 3 for locations of specimens. (a) A2. (b) S1. Pushpin stickers in Fig. 11a and gum in Fig. 11b are markers used for image stitching.

the Brallier and Chemung Formations, across which the greatest amount of structural data is available. For the map-scale contribution, the cross-section is constrained by surface geological contacts and published stratigraphic thicknesses (Reger and Tucker, 1924; Tilton et al., 1927; Dennison, 1963; Dennison and Naegele, 1963; Cardwell et al., 1968; Parker and Heibel, 1993; Schultz, 1995). Structural geometries in the Devonian rocks of the roof sequence are constrained by our field observations and previous work (Reger and Tucker, 1924; Tilton et al., 1927; Dennison, 1963; Ferrill and Dunne, 1989; Johnston, 1989; Schultz, 1995). For the blind duplexes of Cambro–Ordovician carbonates, depth estimates for the floor thrust were based on regional cross-sections (Kulander and Dean, 1986; Mitra, 1986; Wilson and Shumaker, 1988, 1992; Dunne, 1996; Smart et al., 1997), and published seismic-reflection data were used to constrain both the thickness (8000′, or ~2400 m) and geometry of the carbonates (Wilson and Shumaker, 1992).

For the Brallier and Chemung Formations, the cross-section was constructed with dip domains as was done with the profiles and composite profiles in the roof sequence (Suppe, 1983). However, underlying Devonian, Silurian, and Ordovician rocks are known to fold at different scales

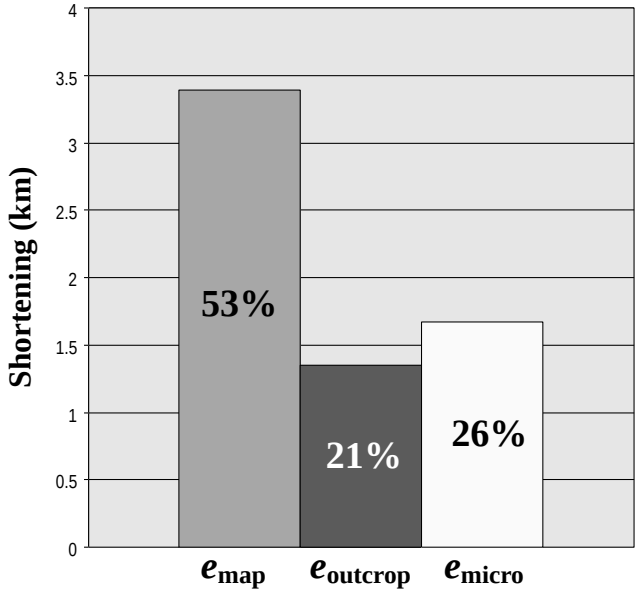

Fig. 12. Summary of strain magnitudes as a function of scale for composite profiles in Fig. 9.

with different styles (Dennison, 1963; Nickelsen, 1963; Gerritson, 1988; Ferrill and Dunne, 1989; Meyer and Dunne, 1990; Scott and Dunne, 1990; Markley and Wojtal, 1996). Therefore, projections of roof-sequence folds below the Devonian rocks are simplified as compared with the likely structures due to the lack of detailed structural information in this stratigraphic interval. The simplification does not invalidate this exercise because the better-constrained Devonian rocks are the focus for this analysis in the roof sequence.

The Ordovician Martinsburg Formation is treated as a weak unit because it is composed dominantly of shales and because it is a regional decollement horizon for the roof thrust of the duplexes containing Cambro–Ordovician carbonates (Gwinn, 1970; Rowlands and Kanes, 1972; Jacobeen and Kanes, 1974; Wiltschko and Chapple, 1977; Perry, 1978a; Evans, 1989). The Cambro–Ordovician carbonates were treated as a stiff unit deformed by fault-bend folds. Thickness was preserved except in the hanging wall ramp beneath the Wills Mountain and Cacapon Mountain anticlines (Evans, 1989; Wilson and Shumaker, 1992).

Plane strain is assumed for the cross-section. Very little evidence exists in the region for a non-plane Alleghanian deformation history (Woodward et al., 1986; Markley and Wojtal, 1996). Data from this study and adjacent work (Ferrill and Dunne, 1989; Johnston, 1989) show consistent shortening directions, which are interpreted as evidence for plane strain.

3.4.2. Spatial distribution of roof-sequence shortening

The Wills Mountain thrust sheet forms a duplex with a flat on flat geometry in the carbonates under the Wills Mountain anticlinorium (Mitra, 1986), whereas the Whip Cove thrust sheet only partially duplicates the carbonates by about 30%. The roof sequence above these two thrust sheet geometries was examined to see if the sequence deformed an equivalent amount in each case (Wills Mountain anticlinorium, zones C–F; Broadtop synclinorium, zones H–J; Fig. 13, Appendix C).

Mapscale shortening in the roof sequence was determined by a line-length calculation at the contact between the Brallier and Chemung Formations (Dahlstrom, 1969, 1970; Ramsay and Huber, 1984), and the carbonate duplex was area balanced (Mitra and Namson, 1989). For the roof sequence, l_{map} is 17.2 km and 18.2 km for anticlinorium and

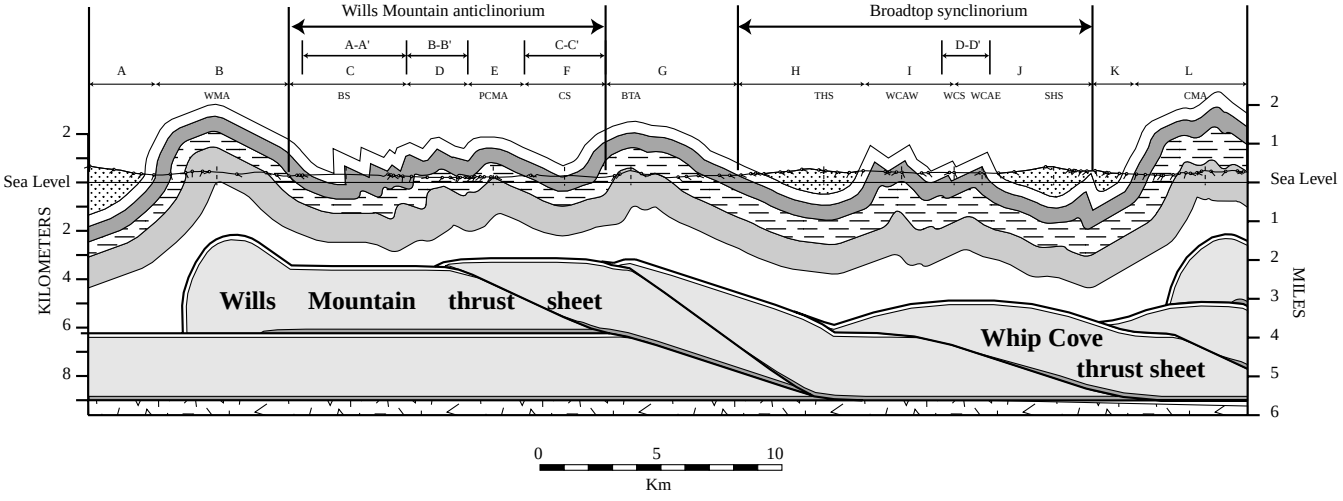

Fig. 13. Regional cross-section through study area. See Figs. 2 and 3 for location. The projected locations of profiles A–A′, B–B′, C–C′, and D–D′ and the Wills Mountain and Broadtop study areas are above the section. Letters A–L show subdivision into zones for regional analysis of submapscale structures (see Appendix C). Lithostratigraphic ornamentation is the same as Fig. 3 for Oswego Formation and younger rocks and the same as Fig. 4 for older rocks; faults = thick black lines; WMA = Wills Mountain anticline; BS = Bedford syncline; PCMA = Patterson Creek Mountain anticline; CS = Clearville syncline; BTA = Broadtop anticline; THS = Town Hill syncline; WCAW = Whip Cove anticline (West); WCS = Whip Cove syncline; WCAE = Whip Cove anticline (East); SHS = Sideling Hill syncline; CMA = Cacapon Mountain anticline.

Table 3
Shortening estimates of roof sequence (Ordovician Oswego Formation and younger) versus Cambro–Ordovician carbonates

	Δl_{map} (km)	$\Delta l_{outcrop}$ (km)	Δl_{micro} (km)	l_1 (km)	l_0 (km)	Shortening km (%)
Wills Mountain anticlinorium study area						
Roof sequence	4.1	1.1	1.2	13.1	19.5	6.4 (32.8%)
Carbonates	13.7	–	–	13.1	26.8	13.7 (51.1%)
					Imbalance (km):	7.3
Broadtop synclinorium study area						
Roof sequence	3.5	1.1	3.6	14.7	22.9	8.2 (35.8%)
Carbonates	5.5	–	–	14.7	20.2	5.5 (27.2%)
					Imbalance (km):	− 2.7
Entire section						
Roof sequence	13.2	4.7	7.7	47.9	73.5	25.6 (34.8%)
Carbonates	35.0	–	–	47.9	82.9	35.0 (42.2%)
					Imbalance (km):	9.4

synclinorium, respectively. For the carbonates, l_{map} is 26.8 km and 20.2 km, respectively (Appendix C, Table 3).

Outcrop-scale shortening estimates were determined for the roof sequence of the cross-section by dividing the section into zones (Fig. 13). For each zone:

$$\text{Outcrop} - \text{scale shortening} = [l_{map}/(1.00 - e_{outcrop})] - l_{map} \quad (5)$$

where l_{map} is the undeformed mapscale line length, and $e_{outcrop}$ is the shortening percentage attributed to outcrop-scale structures.

In the anticlinorium, three of the four zones match composite profiles, so those shortening estimates are used (Fig. 13, Appendix C, Table 3). Zone E is between B–B′ and C–C′ and, therefore, an average value from them of 4.8% was used (Appendix C, Table 3). In the synclinorium, two zones (I and J) partially overlap with D–D′ (Fig. 13). These two zones and zone H were assigned the same outcrop-scale shortening value as D–D′, because D–D′ is the only composite profile from the synclinorium. The outcrop-scale shortening in anticlinorium and synclinorium is 1.1 km (Appendix C, Table 3).

Microscale data from Appendix A were incorporated into the same zones using Eq. (4). The anticlinorium zones were all assigned a LPS of 6.1% (the average LPS of crinoid samples A1–A4 in Appendix A), and the synclinorium zones were assigned a LPS of 13.7% west of the Whip Cove anticline (East) fold axis, and 20.0% east of the fold axis. Calculated shortening values for the anticlinorium and synclinorium are 1.2 km and 3.6 km, respectively.

An imbalance exists in both study areas when summing all three scales of deformation for the roof sequence and comparing them with the mapscale deformation for the carbonates (Table 3, Fig. 14a and b). For the anticlinorium, the roof sequence contains 53% less shortening (7.3 km) than the carbonates directly beneath. Conversely, the synclinorium has an excess of shortening, because it contains 49% more shortening than the underlying carbonates. Consequently, roof-sequence shortening magnitudes do not correlate vertically to the magnitude of duplex duplication, and in fact, shortening magnitude in the synclinorium is relatively greater than in the anticlinorium (Table 3, Fig. 14a and b).

3.4.3. Roof-sequence versus carbonate shortening across region

Having identified opposite vertical shortening imbalances for the anticlinorium and synclinorium, the issue to be addressed with the entire section is whether or not an overall imbalance exists. Outcrop-scale shortening values for the remaining zones (A, B, G, K, and L) were inferred by identifying similarities of the structural geometry and position between these zones and either composite profiles or adjacent study areas (Ferrill and Dunne, 1989; Adamson, 1992; Smart et al., 1997). Similarity was used to justify selection of an outcrop-scale shortening value (Appendix C).

Zones A and K are portions of synclines and so the outcrop-scale shortening estimate from zone F could be applied, but major blind horses end immediately to the hinterland of zones A and K, which is not the case for the Clearville syncline in zone F. To determine a percentage for outcrop-scale shortening in these two zones, the Chemung and Brallier Formations were inspected in a detailed cross-section along strike of zone A (Adamson, 1992). After removing the contribution of the mapscale structures in the same manner as for the composite profiles, an outcrop-scale shortening magnitude of about 11.5% was estimated and applied to zone A. Zone K is structurally analogous to zone A so the same shortening value was applied there.

Zones B, G, and L are all anticlines. Zone G is above the Wills Mountain duplex and between zones F and H, which are also above the duplex. Zone G also contains the Broadtop anticline, which is in the bounding structure between the Wills Mountain anticlinorium and the Broadtop synclinorium. Given the underlying lateral continuity and the surficial boundary position, the outcrop-scale shortening

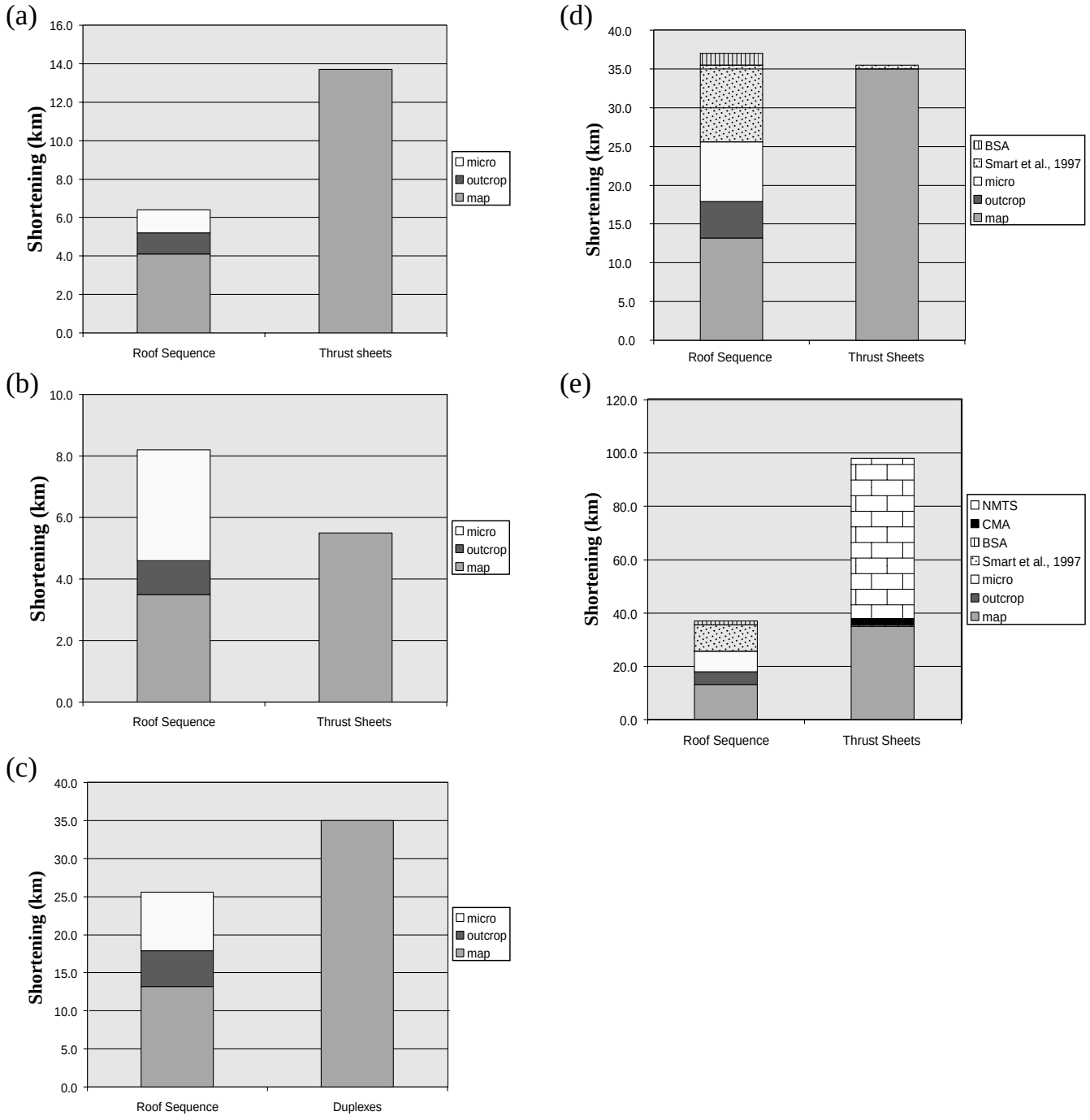

Fig. 14. (a) Comparison of shortening between roof-sequence and thrust sheets for the Wills Mountain anticlinorium (Fig. 13). (b) Comparison of shortening between roof-sequence and thrust sheets for the Broadtop synclinorium. (c) Comparison of shortening between roof-sequence and thrust sheets for Fig. 13. (d) Comparison of shortening between roof-sequence and thrust sheets for Fig. 13 plus data collected in the Appalachian Plateau from Smart et al. (1997) and Woodward (1959). (e) Comparison of shortening between roof-sequence and thrust sheets for Fig. 13 plus data collected in the Appalachian Plateau from Smart et al. (1997) and Woodward (1959), and displacement data from Evans (1989). BSA = Burning Springs anticline; NMTS = North Mountain Thrust Sheet.

value for zone G is an average of the values for zones F and H.

Zones B and L are above hanging wall ramps with significant internal deformation (Wilson and Shumaker, 1992) and must be treated separately from zone G. Previous work by Ferrill and Dunne (1989) in the Devonian Oriskany Sandstone along strike to the southwest from zone L estimated a 15% submapscale shortening contribution. Assuming the submapscale shortening at the Brallier–Chemung contact to be equivalent, a 15% submapscale shortening is ascribed to zone L, and arbitrarily divided equally between outcrop- and microscale based on their regional contributions

(Appendix B). By analogy, the same values are applied to zone B.

Regional microscale shortening was estimated by inferring strain values for zones A, B, G, K, and L (Fig. 13). Zone A was assigned a LPS of 12.2%, which is based on strain ratios calculated from crinoid-bearing sandstones collected in the Chemung Formation along strike to the south in the Appalachian Plateau (Smart et al., 1997). Zones B and L were assigned 7.5% as previously described, zone G is again an average of F and H values, and zone K is adjacent to the samples from zone I with the larger LPS magnitudes, so zone K was assigned its higher strain value of 20% (Appendix C).

The total shortening in the roof sequence at the level of the Brallier and Chemung Formations is 25.6 km (34.8%) versus 35.0 km (42.2%) for the duplex of Cambro–Ordovician carbonates (Table 3, Fig. 14c). The shortening imbalance between these two levels is 9.4 km, which would be an underestimate if any submapscale deformation occurs in the carbonates. Previous workers have inferred that submapscale shortening in the carbonates is probably less than 5%, which could only produce 2–4 km of additional shortening at that level, depending on whether deformation is volume constant or by total volume loss (Ferrill and Dunne, 1989; Evans and Dunne, 1991; Wu, 1993; Dunne 1996). To eliminate the imbalance, the absolute shortening error would need to be 7.4% at the submapscale, but, since 26% of the section has been directly measured rather than inferred, the absolute error would need to be nearly 10% for the remainder of the section. Consequently, we interpret the shortening imbalance to be real and not an artifact of errors in assigning shortening values to the zones in Fig. 13. If only mapscale structures were considered for the roof sequence, a shortening imbalance of 21.8 km would exist between the roof sequence and duplexes (Table 3, Fig. 14c). Incorporating submapscale structures adds an additional 4.4 km at the outcrop-scale and 8.0 km at the microscale, reducing the disparity by 12.4 km (Table 3, Fig. 14c). Consequently, failing to incorporate these data causes a 132% error as compared with the imbalance of 9.4 km (Table 3, Fig. 14c).

4. Discussion

4.1. Implications of considering outcrop-scale structures

4.1.1. Deformation timing as a function of scale

The first implication from considering outcrop-scale structures is that one gains a sense of the relative timeframe in which the roof sequence deformed with respect to duplex formation. For the composite profiles, outcrop-scale shortening is consistently 4–6% except for the 10% in B–B′. Conversely, microscale LPS decreases northwestward from the synclinorium to the anticlinorium. These different spatial distributions of shortening are interpreted to reflect the timing and location of causative shortening events.

For this discussion, we assumed a forelandward imbrication sequence in the duplex and forethrusting in the roof sequence during duplex formation, which are kinematic behaviors commonly attributed to the central Appalachian foreland of the Alleghanian thrust belt (Perry, 1978b; Geiser, 1988a,b; Ferrill and Dunne, 1989; Smart et al., 1997). For forethrusting, bedding in the roof sequence is typically subhorizontal forelandward of the moving thrust sheet, thus subhorizontal shortening in the roof sequence produces LPS. For such a case, the expectation would be that the greatest shortening would be found in the roof sequence in front of horses with larger displacements (e.g. Broadtop synclinorium). Such a strain distribution is found for microscale shortening, but not for outcrop-scale shortening.

If the outcrop-scale folds were attributed to forethrusting-related LPS, they would form during a pure shear and should be symmetric (Marshak and Engelder, 1985; Geiser, 1988a). Yet, both outcrop- and mapscale folds in the composite profiles have asymmetric limb lengths. They lack evidence for hinge migration or selective limb deformation such as slickenlines through fold hinges, veins from tangential longitudinal strain in a limb rather than hinges, or preferential concentration of smaller structures in limbs that dip southeast instead of northwest, or vice versa (Gray, 1981; Mitchell and Woodward, 1988). Thus, the folds are interpreted to be originally asymmetric and not time-equivalent to forethrusting-related LPS.

Based on the spatial distribution of strain magnitudes, the microscale strain is interpreted to be forethrusting related. In contrast, the folds are interpreted to postdate LPS. They have a different spatial distribution for shortening, are asymmetric, and lack the thickened subhorizontal limbs and attenuated subvertical limbs that would result from shape modification by a regional subhorizontal shortening after folding.

Given that the host folds postdate LPS, that outcrop-scale fold symmetry is consistent with their host folds, and that the host folds reflect duplex topography; the outcrop-scale folds are interpreted as having formed as duplex topography developed under them. They probably represent local perturbations during the formation of the host folds by layer-parallel shear (Faill, 1969, 1973; Ramsay, 1974; Stewart and Alvarez, 1991).

4.1.2. Vertical shortening imbalance versus duplex geometry

Beneath the Wills Mountain anticlinorium is a duplex with a flat-on-flat geometry. As Fig. 14a shows, roof-sequence shortening (32.8%) does not match carbonate shortening (51.8%), when one considers deformation from all three scales of measurement for the roof sequence. By contrast, the carbonate-roof sequence shortening disparity is reversed in the Broadtop synclinorium (Fig. 14b). The roof-sequence shortening (35.8%) is actually higher than the shortening of the underlying partially overlapping duplexes

(27.2%). The relatively larger value in the roof sequence of the synclinorium forelandward of the Cacapon Mountain duplex versus the relatively smaller value in the anticlinorium over the Wills Mountain duplex is further support for the occurrence of forethrusting during blind thrusting. This result relates to the fact that microscale shortening shows much greater spatial variation than the outcrop-scale shortening. Thus, while outcrop-scale structures are not a contributor to this effect, measuring their contribution was necessary to establish this relationship.

4.1.3. Regional kinematic interplay between roof sequence and duplexes

This study identifies a shortening imbalance between roof sequence and duplex of about 9.4 km (Table 3). Previous work further into the foreland of the Appalachian Plateau offers a solution to this imbalance. In the foreland of the Wills Mountain duplex, a 9.9 km shortening surplus was identified for the Chemung Formation with respect to underlying Cambro–Ordovician carbonates (Smart et al., 1997). Also, additional shortening of about 1.5 km exists at the Devonian level even further into the foreland of the Appalachian Plateau at the Burning Springs anticline (Woodward, 1959; Gwinn, 1964; Calvert, 1983). Therefore, if these surpluses are interpreted to be the result of forethrusting, they eliminate the shortening imbalance found in this study (Fig. 14d). Still, if outcrop-scale structures were ignored in this study and the work of Smart et al. (1997), then a shortening deficit of 5.6 km would exist in the roof sequence. Such deficits have typically been interpreted as evidence for backthrusting (Banks and Warburton, 1986), which would be an incorrect kinematic interpretation due to a failure to include shortening data from all scales of deformation.

4.1.4. Implications for displacement transfer for a regional thrust sheet

The North Mountain thrust (NMT, Fig. 2) is the base of the North Mountain thrust sheet (NMTS), which has about 60 km of displacement (Evans, 1989). A continuing regional controversy has been whether this displacement is transferred along a blind flat in the Martinsburg Formation into the Valley and Ridge and Plateau (Kulander and Dean, 1986; Dean et al., 1990; Wu, 1993, 1995), or up a ramp through the present surface trace of the NMT (Evans, 1989; 1990; Dunne and Ferrill, 1995; Dunne, 1996). The contribution of the present study to this controversy is to identify the lack of a shortening imbalance between roof sequence and underlying duplex in much of the Valley and Ridge and Plateau provinces. Given this lack of imbalance, if the 60 km of displacement for the NMTS was transferred northwest by a blind flat in the Martinsburg Formation to the northwest, the deformation in the roof sequence must be concentrated in the 30 km interval between the southeast end of Fig. 13 and the surface trace of the NMT (Fig. 2) to accommodate the current imbalance (Fig. 14e). It remains for future work to identify whether the needed 67% additional shortening over this 30 km interval exists. If such an atypical shortening magnitude exists in that region, the results of this study would indicate that outcrop-scale structures should have a prominent role. Their relative abundance might also be an effective simple indicator of the presence or absence of this needed shortening.

4.2. Magnitude of outcrop-scale shortening and relationship to fractal analysis

This study shows that outcrop-scale deformation accounts for about 17–25% of the total shortening ($e_{maxo}/(e_{maxo+m+mi})$ in the roof-sequence in this portion of the Alleghanian foreland thrust belt, or an absolute shortening magnitude of about 6.0% ($e_{maxo}/(l_1 + e_{maxo+m+mi})$) (Appendix B). Wu (1993) predicted that an outcrop-scale shortening magnitude of about 10% would exist above Cacapon Mountain anticline and in the eastern Broadtop synclinorium. One interpretation of the difference between measured values for outcrop-scale shortening and Wu's prediction is that folds do not partition shortening fractally as a function of size. Such an interpretation, however, does not allow for the facts that Wu's analysis was not applied at exactly the same stratigraphic level in the roof sequence, and it used a cross-section that incorporated a multitude of nonexistent mapscale faults (Dean et al., 1985). Thus, a better test of Wu's hypothesis that strain does partition fractally for different size folds would be to use the data in Figs. 6, 7, 9 and 13, and the additional profiles from this study (Hogan, 2000) to construct and test an outcrop-scale prediction. Also, as demonstrated by Wilson (1997), the compass method and not spectral analysis should be used for this new test. Such a test is beyond the scope of the present work.

5. Conclusions

1. Outcrop-scale deformation in the Upper Devonian Chemung–Brallier Formation boundary contributes about 17–25% of the total shortening in this portion of the Alleghanian foreland thrust belt (Figs. 9 and 12). Collectively, the magnitude of shortening is nearly equal to the microscale-shortening contribution for the composite profiles analyzed in this study, but microscale shortening shows a much greater variation across the study area, whereas outcrop-scale shortening is relatively constant.
2. The submapscale shortening components equal the mapscale shortening that would be interpreted from a regional cross-section. Failure to incorporate submapscale shortening would cause the following errors: misrepresentation of overall kinematic interaction between roof sequence and duplex, and inaccurate assessment of

Appendix A

The following table shows shortening data from deformed crinoids in the Chemung Formation.

Sample no.	No. of measured ossicles	Bedding orientation[a]	Harmonic mean of R_s	Mean ϕ trend	Shortening direction[b]	e_{micro} (%)
Wills Mountain anticlinorium						
A1	36	026/14	1.05 ± 0.04	028 ± 21°	118°	0.048 (4.8)
A2	36	029/16	1.07 ± 0.05	015 ± 21°	105°	0.065 (6.5)
A3	25	030/20	1.06 ± 0.05	025 ± 29°	115°	0.057 (5.7)
A4	32	224/41	1.08 ± 0.06	049 ± 21°	139°	0.074 (7.4)
				Average:	119 ± 10°	0.061 (6.1 ± 0.9)
Broadtop synclinorium						
S1	45	032/53	1.14 ± 0.09	033 ± 20°	123°	0.123 (12.3)
S2	41	202/25	1.15 ± 0.07	227 ± 18°	137°	0.130 (13.0)
S3	49	020/81	1.08 ± 0.06	018 ± 25°	108°	0.074 (7.4)
S4	43	028/26	1.18 ± 0.07	358 ± 15°	088°	0.153 (15.3)
S5	42	202/64	1.23 ± 0.08	359 ± 15°	089°	0.187 (18.7)
S6	9	026/52	1.21 ± 0.06	031 ± 12°	121°	0.174 (17.4)
S7	21	027/56	1.31 ± 0.09	035 ± 10°	125°	0.237 (23.7)
S8	31	027/56	1.25 ± 0.11	041 ± 15°	131°	0.200 (20.0)
				S1–S4 Average:	114 ± 16°	0.120 (12.0 ± 2.3)
				S5–S8 Average:	117 ± 14°	0.200 (20.0 ± 1.9)

[a] Righthand rule format for bedding orientations.
[b] Calculated as perpendicular to mean ϕ trend.

Appendix B

The following table shows a summary of strain magnitudes for composite profiles in Fig. 9.

Profile	Mapscale shortening Δl_{maxm}, Δl_{minm} (e_{maxm}, e_{minm})[b]	Outcrop-scale shortening $\Delta l_{maxo>}$, Δl_{mino} (e_{maxo}, e_{mino})	Microscale shortening Δl_{maxmi}, Δl_{minmi} (e_{maxmi}, e_{minmi})	l_{0max}, l_{0min}	l_1	Total shortening (%)[a]	
						$e_{maxo+m+mi}$	$e_{mino+m+mi}$
A–A′	1.64, 1.59 (63%, 63%)	0.45, 0.45 (17%, 18%)	0.50, 0.49 (20%, 19%)	8.15, 8.09	5.56	2.59 (31.8%)	2.53 (31.3%)
B–B′	0.51, 0.34 (30%, 40%)	0.47, 0.50 (45%, 37%)	0.29, 0.28 (25%, 23%)	4.70, 4.55	3.43	1.18 (25.6%)	1.12 (24.6%)
C–C′	0.22, 0.18 (35%, 31%)	0.16, 0.17 (25%, 29%)	0.25, 0.24 (40%, 40%)	4.05, 4.01	3.42	0.63 (15.6%)	0.59 (14.7%)
D–D′	1.02, 0.74 (53%, 46%)	0.27, 0.27 (14%, 17%)	0.63, 0.59 (33%, 37%)	4.60, 4.28	2.68	1.92 (41.7%)	1.60 (37.4%)
Total:	3.39, 2.85 (53%, 49%)	1.35, 1.39 (21%, 24%)	1.67, 1.60 (26%, 27%)	21.41, 20.93	15.09	6.32 (29.5%)	5.84 (27.9%)

[a] Total shortening is a distance in kilometers with a percentage for absolute shortening magnitude.
[b] Shortening is a distance in kilometers with a percentage for relative contribution to total shortening.

Appendix C

The following table shows a summary of strain assessments in the roof sequence of cross-section line 13. See Figs. 2 and 3 for location.

Zone	l_1	l_{map}	Mapscale shortening		Outcrop-scale shortening		l_{o+m}	Microscale shortening		l_{o+m+mi}	Total shortening
	(km)	(km)	e_{map}	Δl in km (e in %[a])	$e_{outcrop}$	Δl in km (e in %[a])	(km)	e_{micro}	Δl in km (e in %[a])	(km)	Δl in km (e in %[a])
A	2.8	3.7	0.188	0.9 (18.8)	0.115	0.5 (10.5)	4.2	0.122	0.6 (12.2)	4.8	2.0 (41.5)
B	5.5	7.3	0.211	1.8 (21.1)	0.075	0.6 (7.0)	7.9	0.075	0.6 (7.5)	8.5	3.0 (35.6)
C	4.8	7.4	0.313	2.6 (31.3)	0.055	0.4 (4.8)	7.8	0.061	0.5 (6.1)	8.3	3.5 (42.2)
D	2.6	3.1	0.138	0.5 (13.8)	0.101	0.3 (8.3)	3.4	0.061	0.2 (6.1)	3.6	1.0 (28.2)
E	2.3	2.7	0.130	0.4 (13.0)	0.056	0.2 (6.5)	2.9	0.061	0.2 (6.1)	3.1	0.8 (25.6)
F	3.3	4.1	0.175	0.8 (17.5)	0.040	0.2 (4.4)	4.3	0.061	0.3 (6.1)	4.6	1.3 (28.0)
G	5.5	6.0	0.072	0.5 (7.2)	0.048	0.3 (4.3)	6.3	0.099	0.7 (9.9)	7.0	1.5 (21.4)
H	5.5	6.4	0.114	0.9 (11.4)	0.056	0.4 (5.1)	6.8	0.137	1.1 (13.7)	7.9	2.4 (30.2)
I	4.6	5.8	0.170	1.2 (17.0)	0.056	0.3 (4.2)	6.1	0.137	1.0 (13.7)	7.1	2.5 (34.9)
J	4.6	5.9	0.165	1.3 (16.5)	0.056	0.4 (5.1)	6.3	0.200	1.6 (20.0)	7.9	3.3 (41.6)
K	1.7	2.4	0.207	0.7 (20.7)	0.115	0.3 (8.9)	2.7	0.200	0.7 (20.0)	3.4	1.7 (49.6)
L	4.7	6.3	0.218	1.6 (21.8)	0.075	0.5 (6.8)	6.8	0.075	0.6 (7.5)	7.4	2.7 (36.1)
Total:	47.9	61.1	0.180	13.2 (18.0)	0.060	4.4 (6.0)	65.5	0.108	8.0 (10.8)	73.5	25.6 (34.8)

[a] Percent shortening calculated using l_{o+m+mi}.

the displacement transfer from a thrust with 50 + km of movement. Such kinematic errors would lead to mechanical misunderstandings of the development of this or any tectonic province (e.g. Mitra, 1994).

3. The predicted outcrop-scale shortening from a fractal analysis of fold complexity was not found, but the analysis should be performed on a new data set such as the one in this study to truly test whether fold shortening has a fractal relationship with changing scale.
4. Combining results of this study with previous deformation analysis in Devonian rocks of the Appalachian Plateau, the 60 + km of displacement transfer from the NMT is absent. If the transfer is present in the tectonic province, it must lie hinterlandward of the study area and require an atypical shortening magnitude in the roof sequence of +65%.
5. Evidence for regional forethrusting from this study includes: large microscale shortening magnitudes forelandward of the Cacapon Mountain duplex, larger overall strain values in the Broadtop synclinorium compared with the Wills Mountain anticlinorium, and roof sequence shortening in the synclinorium exceeding shortening by the underlying carbonate horse. These results support previous kinematic interpretations from the region for forethrusting behavior in the roof sequence.

Acknowledgements

This work was conducted as partial fulfillment of a Masters Degree at the University of Tennessee. We would also like to thank Sigma Xi, Southeastern-section Geological Society of America, the National Geological Society of America and the University of Tennessee SARIF EPPE fund for financial support. Reviews by David Gray, Steven G. Driese and Robert D. Hatcher, Jr. improved this manuscript. Lastly, Art Schultz of the USGS is thanked for providing numerous data locations, maps, and lithostratigraphic interpretations.

References

Adamson, G.W., 1992. Fold development in the cover enveloping the Broadtop horse. M.S. thesis, West Virginia University.

Allmendinger, R.W., 1992. Fold and thrust tectonics of the western United States exclusive of the accreted terranes. In: Burchfiel, B.C., Lipman, P.W., Zoback, M.L. (Eds.). The Cordilleran Orogen: Conterminous U.S. The Geology of North America G-3, pp. 553–581.

Banks, C.J., Warburton, J., 1986. 'Passive roof' duplex geometry in the frontal structures of the Kirthar and Sulaiman mountain belts, Pakistan. Journal of Structural Geology 8, 229–237.

Boyer, S.E., Elliott, D., 1982. Thrust systems. American Association of Petroleum Geologists Bulletin 66, 1196–1230.

Burgmann, R., 1991. Transpression along the southern San Andreas fault, Durmid Hill, California. Tectonics 10, 1152–1163.

Calvert, G., 1983. Subsurface structure of the Burning Springs anticline, West Virginia — evidence for a two-stage structural development. Proceedings of the Appalachian Basin Industrial Associates 4, 147–164.

Cardwell, D.H., Erwin, R.B., Woodward, H.P., Lotz, C.W., 1968. 1968 Geologic Map of West Virginia. West Virginia Geological and Economic Survey, scale 1:250,000.

Cloos, E., 1947. Oolite deformation in the South Mountain fold, Maryland. Geological Society of America Bulletin 58, 843–918.

Cloos, E., 1951. Structural geology of Washington County. In: The Physical Features of Washington County: Maryland Department of Geology, Mines, and Water Resources Report 14, 124–163.

Dahlstrom, C.D.A., 1969. Balanced cross-sections. Canadian Journal of Earth Science 6, 743–757.

Dahlstrom, C.D.A., 1970. Structural geology in the eastern margin of the Canadian Rocky Mountains. Bulletin of Canadian Petroleum Geology 18, 332–406.

Dahlstrom, C.D.A., 1990. Geometric constraints derived from the law of conservation of volume and applied to evolutionary models for detachment folding. American Association of Petroleum Geologists Bulletin 74, 336–344.

Dean, S.L., Kulander, B.R., Lessing, P., 1985. Geology of the Capon Springs, Mountain Falls, Wardensville, Woodstock, and Yellow Springs Quadrangles, Hampshire and Hardy Counties, West Virginia. West Virginia Geological and Economic Survey WV-26, Morgantown, West Virginia.

Dean, S.L., Kulander, B.R., Lessing, P., 1990. The structural geometry and evolution of foreland thrust systems, northern Virginia: alternative interpretation and reply. The Geological Society of America Bulletin 102, 1442–1445.

Dennison, J.M., 1963. Geology of the Keyser quadrangle. West Virginia, Maryland. West Virginia Geological and Economic Survey, scale 1:24,000.

Dennison, J.M., 1971. Petroleum related to Middle and Upper Devonian deltaic facies in central Appalachians. American Association of Petroleum Geologists Bulletin 55, 1179–1193.

Dennison, J.M., Naegele, O.D., 1963. Structure of Devonian strata along Allegheny Front from Corriganville, Maryland, to Spruce Knob, West Virginia. West Virginia Geological and Economic Survey Bulletin, 24.

Dennison, J.M., Barrell, S.M., Warne, A.G., 1988. Northwest–southeast cross-section of Devonian Catskill delta in east-central West Virginia and adjacent Virginia. In: Dennison, J.M. (Ed.). Geologic Field Guide to Devonian Delta East-central West Virginia and Adjacent Virginia. American Association of Petroleum Geologists Eastern Section Meeting, pp. 12–36.

Dixon, J.S., 1982. Regional structural synthesis, Wyoming salient of western overthrust belt. The American Association of Petroleum Geologists Bulletin 66, 1560–1580.

Donn, W.L., Shimer, J.A., 1958. Graphic Methods in Structural Geology. Appleton Century-Crofts, New York.

Dubey, A.K., Cobbold, P.R., 1977. Noncylindrical flexural slip folds in nature and experiment. Tectonophysics 38, 223–239.

Dunne, W.M., 1996. The role of macroscale thrusts in the deformation of the Alleghanian roof sequence in the central Appalachians: a reevaluation. American Journal of Science 296, 549–575.

Dunne, W.M., Ferrill, D.A., 1995. Fractal strain distribution and its implications for cross-section balancing: discussion. Journal of Structural Geology 17, 757–760.

Engelder, T., 1979a. Mechanisms for strain within the Upper Devonian clastic sequence of the Appalachian Plateau, western New York. American Journal of Science 279, 527–542.

Engelder, T., 1979b. The nature of deformation within the outer limits of the central Appalachian foreland fold and thrust belt in New York State. Tectonophysics 55, 289–310.

Epard, J., Groshong, R.H., 1993. Excess area and depth to detachment. The American Association of Petroleum Geologists Bulletin 77, 1291–1302.

Evans, M.A., 1989. The structural geology and evolution of foreland thrust

systems, northern Virginia. Geological Society of America Bulletin 101, 339–354.
Evans, M.A., 1990. The structural geometry and evolution of foreland thrust systems, northern Virginia: alternative interpretation and reply. The Geological Society of America Bulletin 102, 1442–1445.
Evans, M.A., Dunne, W.M., 1991. Strain factorization and partitioning in the North Mountain thrust sheet, central Appalachians, USA. Journal of Structural Geology 13, 21–35.
Faill, R.T., 1969. Kink band structures in the Valley and Ridge Province, central Pennsylvania. Geological Society of America 80, 2539–2550.
Faill, R.T., 1973. Kink-band folding, Valley and Ridge Province, Pennsylvania. Geological Society of America Bulletin 84, 1289–1314.
Ferrill, D.A., Dunne, W.M., 1989. Cover deformation above a blind duplex: an example from West Virginia, USA. Journal of Structural Geology 11, 421–431.
Ferrill, D.A., Morris, A.P., Jones, S.M., Stamatakos, J.A., 1998. Extensional layer-parallel shear and normal faulting. Journal of Structural Geology 20, 355–362.
Geiser, P.A., 1988a. The role of kinematics in the construction and analysis of geological cross-sections in deformed terranes. In: Mitra, G., Wojtal, S. (Eds.). Geometries and Mechanisms of Thrusting, with Special Reference to the Appalachians. Special Paper to the Geological Society of America 222, pp. 47–76.
Geiser, P.A., 1988b. Mechanisms of thrust propagation: Some examples and implications for the analysis of overthrust terranes. Journal of Structural Geology 10, 829–845.
Gerritson, S.S., 1988. Structural analysis of the Silurian–Devonian cover in the Smoke Holes, West Virginia. M.S. Thesis, West Virginia University.
Gray, D.R., 1981. Cleavage-fold relationships and their implications for transected folds: an example from southwest Virginia, USA. Journal of Structural Geology 3, 265–277.
Groshong, R.H., 1972. Strain calculated from twinning in calcite. Geological Society of America Bulletin 83, 2025–2037.
Gwinn, V.E., 1964. Thin-skinned tectonics in the Plateau and northwestern Valley and Ridge provinces of the central Appalachians. Geological Society of America Bulletin 75, 863–900.
Gwinn, V.E., 1970. Kinematic patterns and estimates of lateral shortening, Valley and Ridge and Great Valley provinces, central Appalachians, south-central Pennsylvania. In: Fisher, G.W., Pettitjohn, F.J., Reed Jr, J.C., Weaver, K.N. (Eds.). Studies of Appalachian Geology, Central and Southern. Wiley-Interscience, New York, pp. 127–146.
Hancock, P.L., 1985. Brittle microtectonics: principles and practice. Journal of Structural Geology 7, 437–457.
Hatcher Jr, R.D., 1981. Thrusts and nappes in the North American Appalachian Orogen. In: McClay, K.R., Price, N.J. (Eds.). Thrust and Nappe Tectonics. Geological Society Special Publication 9, pp. 491–497.
Hogan, J.P.L., 2000. Calculation of shortening due to outcrop-scale deformation and its relation to regional deformation patterns. M.S. thesis, University of Tennessee, Knoxville.
Holl, J.E., Anastasio, D.J., 1995. Cleavage development within a foreland fold and thrust belt, southern Pyrenees, Spain. Journal of Structural Geology 17, 357–369.
Jacobeen Jr, F., Kanes, W.H., 1974. Structure of the Broadtop synclinorium and its implications for the Appalachian structural style. The American Association of Petroleum Geologists Bulletin 58, 362–375.
Johnston, M.A., 1989. Alleghanian cover strain in the central Appalachians of Maryland and West Virginia. M.S. thesis, West Virginia University.
Kattenhorn, S.A., McConnell, D.A., 1994. Analysis of outcrop-scale fault-related folds, Eagle Rock, Virginia. Southeastern Geology 34, 79–88.
Kligfield, R., Crespi, J., Naruk, S., Davis, G.H., 1984. Displacement and strain patterns of extensional orogens. Tectonics 3, 577–609.
Kulander, B.R., Dean, S.L., 1986. Structure and tectonics of central and southern Appalachian Valley and Ridge and Plateau Provinces, West Virginia and Virginia. The American Association of Petroleum Geologists Bulletin 70, 1674–1684.
Laubscher, H.P., 1962. Die Zweiphasenhypothese der Jurafaltung. Ecolgae Geologicae Helvetiae 55, 1–22.
Laubscher, H.P., 1977. Fold development in the Jura. Tectonophysics 37, 337–362.
Lisle, R.J., 1977. Estimation of tectonic strain variation from the mean shape of deformed elliptical markers. Geologie en Mijnbouw 56, 140–144.
Lisle, R.J., 1985. Geological Strain Analysis. A Manual for the R_f/f Method. Pergamon Press, New York.
Mackin, J.H., 1950. The down-structure method of viewing geologic maps. Journal of Geology 58, 55–72.
Markley, M., Wojtal, S., 1996. Mesoscopic structure, strain, and volume loss in folded cover strata, Valley and Ridge Province, Maryland. American Journal of Science 296, 23–57.
Marshak, S., Engelder, T., 1985. Development of cleavage in limestones of a fold-thrust belt in eastern New York. Journal of Structural Geology 7, 345–359.
Meyer, T.J., Dunne, W.M., 1990. Deformation of Helderberg limestones above the blind thrust system of the Central Appalachians. Journal of Geology 98, 108–117.
Mitchell, M.M., Woodward, N.B., 1988. Kink detachment fold in the southwest Montana fold and thrust belt. Geology 16, 162–165.
Mitra, G., 1994. Strain variation in thrust sheets across the Sevier fold-and-thrust belt (Idaho–Utah–Wyoming): implications for section restoration and wedge taper evolution. Journal of Structural Geology 16, 585–602.
Mitra, S., 1986. Duplex structures and imbricate thrust systems: geometry, structural position, and hydrocarbon potential. The American Association of Petroleum Geologists Bulletin 70, 1087–1111.
Mitra, S., Namson, J., 1989. Equal-area Balancing. American Journal of Science 289, 563–599.
Nair, N.S., 1992. Crinoid deformation and regional structural geology in eastern West Virginia and northwestern Virginia. M.S. thesis, University of Toledo.
Nair, N.S., Dean, S.L., Lessing, P., Kulander, B.R., 1995. Crinoid deformation and sedimentary rock cover shortening in eastern West Virginia and northwestern Virginia. GSA Abstracts with Programs, Southeastern Section, 77.
Nickelsen, R.P., 1963. Fold patterns and continuous deformation mechanisms of the central Pennsylvania folded Appalachians. In: Catem, A. (Ed.). Guidebook: Tectonics and Cambro–Ordovician Stratigraphy, Central Appalachians of Pennsylvania. Pittsburgh Geological Society with the Appalachian Geological Society, pp. 13–29.
Nickelsen, R.P., 1979. Sequence of structural stages of the Alleghany orogeny, at the Bear Valley Strip Mine, Shamokin, Pennsylvania. American Journal of Science 279, 225–271.
Onasch, C.M., 1984. Application of the R_f/f technique to elliptical markers deformed by pressure solution. Tectonophysics 110, 157–165.
Onasch, C.M., Dunne, W.M., 1993. Variation in quartz arenite deformation mechanisms between a roof sequence and duplexes. Journal of Structural Geology 15, 465–475.
Parker, R.A., Heibel, T., 1993. Preliminary Bedrock Geology of Parts of the Burlington, Headsville, Old Fields, Romney, and Springfield Quadrangles, Grant, Hampshire, Hardy, and Mineral Counties, West Virginia. U.S. Geological Survey Open-File Report 93-9, 6 sheets.
Perry, W.J., Jr., 1971. Structural development of the Nittany Anticlinorium, Pendleton County, West Virginia. Ph.D. thesis, Yale University.
Perry Jr, W.J., 1978a. Sequential deformation in the central Appalachians. American Journal of Science 278, 518–542.
Perry, W.J., Jr., 1978. The Wills Mountain anticline: a study in complex folding and faulting in eastern West Virginia: West Virginia Geological and Economic Survey Report of Investigation RI-32, 29pp.
Pumpelly, R., 1918. My Reminiscences. Vol. 2. Henry Holt and Company, New York.
Ramsay, J.G., 1974. Development of chevron folds. Geological Society of America Bulletin 85, 1741–1754.
Ramsay, J.G., 1981. Tectonics of the Helvetic Nappes. In: McClay, K.R.,

Price, N.J. (Eds.). Thrust and Nappe Tectonics. Geological Society Special Publication 9, pp. 293–309.

Ramsay, J.G., Huber, M.I., 1983. The Techniques of Modern Structural Geology. Volume 1: Strain Analysis. Academic Press, London.

Ramsay, J.G., Huber, M.I., 1984. The Techniques of Modern Structural Geology. Volume 2: Folds and Faults. Academic Press, London.

Reger, D.B. Tucker, R.C., 1924. Mineral and Grant Counties. West Virginia Geological Survey County Report 1924, 866pp.

Reks, I.J., Gray, D.R., 1983. Strain patterns and shortening in a folded thrust sheet: an example from the southern Appalachians. Tectonophysics 93, 99–128.

Rodgers, J., 1970. The Tectonics of the Appalachians. Wiley Interscience, New York.

Roeder, D.H., Witherspoon, W.D., 1978. Palinspastic map of east Tennessee. American Journal of Science 278, 543–555.

Rowlands, D., Kanes, W.H., 1972. Structure of the Broadtop synclinorium, a study in seismic, subsurface and surface geology. In: Lessing, P., Hayhurst, R.I., Barlow, J.A., Woodfork, L.D. (Eds.). Appalachian Structures Origin, Evolution, and Possible Potential for New Exploration Frontiers. A Seminar. March 3–5, 1971. West Virginia University and West Virginia Geological and Economic Survey.

Schultz, A., 1995. Geology of the Broadtop synclinorium within the Winchester $30' \times 60'$ quadrangle, West Virginia. U.S. Geological Survey Open-File Report 97-143, 51pp.

Scott, P.B., Dunne, W.M., 1990. Deformation history of an outcrop-scale fault system in the central Appalachians. Southeastern Geology 31, 93–107.

Simon, R.I., Gray, D.R., 1982. Interrelations of mesoscopic structures and strain across a small regional fold, Virginia Appalachians. Journal of Structural Geology 4, 271–289.

Smart, K.J., Dunne, W.M., Krieg, R.D., 1997. Roof sequence response to emplacement of the Wills Mountain duplex: The roles of forethrusting and scales of deformation. Journal of Structural Geology 19, 1443–1459.

Socolow, A.A., 1980. Geologic map of Pennsylvania. Commonwealth of Pennsylvania Department of Environmental Resources Bureau of Topographic and Geologic Survey, scale 1:250,000.

Stanley, R.F., 1990. The evolution of mesoscopic imbricate thrust faults—an example from the Vermont Foreland, USA. Journal of Structural Geology 12, 227–241.

Stewart, I.S., Hancock, P.L., 1991. Scales of structural heterogeneity within neotectonic normal fault zones in the Aegean region. Journal of Structural Geology 13, 191–204.

Stewart, K.G., Alvarez, W., 1991. Mobile-hinge kinking in layered rocks and models. Journal of Structural Geology 13, 243–259.

Suppe, J., 1983. Geometry and kinematics of fault-bend folding. American Journal of Science 283, 684–721.

Tavarnelli, E., Holdsworth, R.E., 1999. How long do structures take to form in transpression zones? A cautionary tale from California. Geology 27, 1063–1066.

Tilton, J.L., Prouty, W.F., Tucker, R.C., Price, P.H., 1927. Hampshire and Hardy Counties. West Virginia Geological Survey County Report 1927.

Weaver, K.N., 1968. Geologic Map of Maryland. Maryland Geological Survey. 1:250,000.

Wernicke, B., 1992. Cenozoic extensional tectonics of the U.S. Cordillera. In: Burchfiel, B.C., Lipman, P.W., Zoback, M.L. (Eds.). The Cordilleran Orogen: Conterminous U.S. The Geology of North America G-3, pp. 553–581.

Wernicke, B., Burchfiel, B.C., 1982. Modes of extensional tectonics. Journal of Structural Geology 4, 105–115.

Williams, P.F., 1970. A criticism of the use of style in the study of deformed rocks. Geological Society of America Bulletin 81, 3283–3296.

Wilson, T.H., 1997. Fractal strain distribution and its implications for cross-section balancing: further discussion. Journal of Structural Geology 19, 129–132.

Wilson, T.H., Shumaker, R.C., 1988. Three dimensional structural interrelationships within Cambrian Ordovician lithotectonic unit of central Appalachians. The American Association of Petroleum Geologists Bulletin 72, 600–614.

Wilson, T.H., Shumaker, R.C., 1992. Broad Top thrust sheet: an extensive blind thrust in the central Appalachians. The American Association of Petroleum Geologists Bulletin 76, 1310–1324.

Wiltschko, D.V., Chapple, W.M., 1977. Flow of weak rocks in Appalachian Plateau folds. The American Association of Petroleum Geologists Bulletin 61, 653–670.

Wojtal, S., 1986. Deformation within foreland thrust sheets by populations of minor faults. Journal of Structural Geology 8, 341–360.

Wojtal, S., 1989. Measuring displacement gradients and strains in faulted rocks. Journal of Structural Geology 11, 669–678.

Woodward, H.P., 1959. Structural interpretations of the Burning Springs anticline. In: Woodward, H.P. (Ed.). The Sandhill Deep Well, Wood County, West Virginia. West Virginia Geological and Economic Survey Report Investigations 18, pp. 159–168.

Woodward, N.B., 1985. Valley and Ridge thrust belt: balanced structural sections, Pennsylvania and Alabama. University of Tennessee Dept. of Geological Sciences: Studies in Geology, 12.

Woodward, N.B., Gray, D.R., Spears, D.B., 1986. Including strain data in balanced cross-sections. Journal of Structural Geology 8, 313–324.

Wu, S., 1993. Fractal strain distribution and its implications for cross-section balancing. Journal of Structural Geology 15, 1497–1507.

Wu, S., 1995. Fractal strain distribution and its implications for cross-section balancing: reply. Journal of Structural Geology 17, 761–764.